BILINGUAL PUBLISHING GROUP

Journal of Building Material Science

https://journals.bilpubgroup.com/index.php/jbms

ARTICLE

Analysis of the Effect of Nonplanarity on Ground Deformation

Piu Kundu

Department of Mathematics, School of Advanced Sciences, VIT-AP University, Inavolu, Beside AP Secretariat, Amaravati 522241, Andhra Pradesh, India

ABSTRACT

The movement of interacting faults within the Earth's crust during earthquakes may cause significant structural damage. Large earthquake fault surfaces are often planar or a combination of several planar fault segments. This study analyses the interaction between a non-planar and a planar fault, where the faults are inclined, buried, creeping and strike-slip in nature. The non-planar fault is infinite and formed by two interconnected planar segments, while the planar fault is finite. The present analysis adduces the movement of interacting faults in a composite structure comprised of an elastic layer nested on a visco-elastic substrate of Maxwell medium. The significant effect of various affecting parameters viz. inclination of the faults, velocity of the fault movement, depth of the faults from the free surface, distance between the faults and the non-planarity of the fault has been discussed and also compared. The amount of stress and surface shear strain is restored after the creeping movement. The graphical representation of the effect of non-planarity of the fault on stress-strain accumulation has been established. Analytical solutions are obtained using Laplace transform and Green's function techniques, supported by numerical simulations. The obtained results provide insights into fault interaction process and have important implications for assessing seismic hazard potential in viscoelastic media. The study of such earthquake fault dynamical models may give some ideas about the nature of stress-strain accumulation or release in the system and help us to observe the mechanism of lithosphere-asthenosphere boundary.

Keywords: Interaction Between Nonplanar and Planar Fault; Creeping Movement; Aseismic Period; Integral Transform; Green's Function Technique

*CORRESPONDING AUTHOR:

Piu Kundu, Department of Mathematics, School of Advanced Sciences, VIT-AP University, Inavolu, Beside AP Secretariat, Amaravati 522241, Andhra Pradesh, India; Email: piukundu91@gmail.com

ARTICLE INFO

Received: 25 June 2025 | Revised: 3 September 2025 | Accepted: 16 September 2025 | Published Online: 28 November 2025
DOI: https://doi.org/10.30564/jbms.v7i4.10418

CITATION

Kundu, P., 2025. Analysis of the Effect of Nonplanarity on Ground Deformation. Journal of Building Material Science. 7(4): 84–111. DOI: https://doi.org/10.30564/jbms.v7i4.10418

1. Introduction

One of the most devastating natural hazards is earthquakes which occur due to the movement of various types of seismic faults with different geometrical structures. Countries like Japan, U.S.A., China and the countries in the middle and the far east have been suffering from destructive earthquakes. The development of earthquake prediction programmes becomes a practical goal of modern research in earthquake seismology. A majority of major earthquakes are tectonic earthquakes occurring due to the release of elastic strain energy accumulated within the subsurface rock in the region over a long period. One of the most significant achievements in modern seismology is the recognition of the fact that most of the major earthquakes, especially the shallow ones, are caused by faults in the earth. A fault is a slip surface in the earth across which discontinuous land movement takes place. The faults are of different types, they can be finite or infinite in length, buried or surface-breaking, creeping or locked and strike-slip or dip-slip in movement. Some of the faults are single while some are interacting. Sierra Madre fault and Raymond fault are single faults whereas Calaveras and Garlock are interacting faults in the neighbourhood of the San Andreas fault. Apart from the geometrical complexity of faults, another crucial factor influencing ground deformation is the distinction between near-field and far-field effects. Near-field deformation is typically characterized by sharp variations in stress and displacement close to the fault, while far-field deformation governs the long-range distribution of strain energy. This concept has been emphasized in Gabbianelli et al.[1] and is particularly relevant for interpreting the implications of the present model. Liu et al.[2] used high resolution InSAR to show that large earthquakes on strike-slip faults can accelerate and prolong shallow creep in viscoelastic materials. Mahato and Sarkar[3] introduced a fractional Standard linear solid framework for interacting faults and demonstrated that creep velocity and fault inclination strongly influence displacement and stress accumulation. Kundu[4] investigated the mutual interaction between infinite and finite faults in a Maxwell viscoelastic half-space, emphasizing the roles of inclination, movement rate, depth and geometric parameters in deformation behaviour. “Ground deformation due to interacting faults” has been described by Kundu and Sarkar (Mondal)[5]. Mondal et al.[6] analyzed the effect of a strike-slip fault of infinite length situated in an elastic layer, which overlies a viscoelastic half-space. Muir et al.[7] have analysed interacting fault models in California and Hindu Kush. Dutta et al.[8] have introduced a method for estimating complex nonplanar earthquake fault geometry. Some of the faults have some nonplanar structures such as the 1999 Izmit, Turkey, earthquake has a nonplanar fault structure. Li and Liu[9] have presented a nonplanar subduction fault model for northern Cascadia. Sen et al.[10] have considered a nonplanar strike-slip fault situated in the viscoelastic half-space of the lithosphere. “Effects of Nonplanar Fault Topology and Mechanical Interaction on Fault-Slip Distributions in the Ventura Basin, California” has been described by Marshall et al.[11]. For demonstrating the effect of fault geometry on slow slip events, Mitsui and Hirahara[12] described slow slip on a fault. The earthquake faults are situated in elastic or viscoelastic medium of Maxwell or standard linear solid or Burger rheology. The analysis of earthquake fault movement in elastic medium has been illustrated by Rani et al.[13,14], Rybicki[15], Maruyama[16,17], Chinnery[18,19] and Steketee[20].

Although several studies have previously investigated interacting faults[5,6] and non-planar fault geometries[10], the present work differs in several important aspects. First, unlike Kundu et al.[5] and Mondal et al.[6], which primarily considered planar fault interactions in layered media, our model introduces the interaction between a buried, infinite non-planar strike-slip fault and a finite planar fault, thereby incorporating geometric complexity absent in earlier formulations. Second, while Sen[10] examined a single non-planar fault in a viscoelastic half-space, we extend the analysis by including fault-fault interactions within a composite structure consisting of an elastic layer over a Maxwell viscoelastic substrate. Third, the present study develops closed-form analytic solutions using Laplace transform and Green’s function techniques, which allow us to capture both transient and long-term deformation behaviour more explicitly than most prior numerical approaches. Finally, the physical implications are examined not only through stress and strain accumulation but also through quantitative comparison with real earthquske observations (e.g., the 2008 Wenchuan earthquake) and benchmark models such as Duan and Oglesby[21]. These distinctions highlight the original contribution of this study in advancing the understanding of ground deformation

due to complex fault interactions.

Due to high temperature and pressure, the results of the laboratory experiment on rocks simulating the conditions in the lower lithosphere and asthenosphere also indicate that at a temperature and pressure which is expected in the lithosphere and asthenosphere, rheological behaviour of rocks is likely to be brittle elastic in the upper lithosphere and soft imperfectly elastic in the asthenosphere. With these points in view, lithosphere-asthenosphere system has been represented by an elastic layer overlying a viscoelastic half-space. To the best of the author's knowledge, based on the reviewed literature, no investigation has been conducted to analyze the effect of an interacting fault model situated in an elastic stratum overlying a viscoelastic substrate. The interaction between nonplanar and planar faults can be regarded as a novel feature of the present investigation. These facts serve as the motivation for the authors to explore the effect of ground deformation due to interaction between the faults of nonplanar and planar structure. In the present investigation, for analysing aseismic ground deformation, we have developed an interacting fault model of an infinite nonplanar fault and a planar fault of finite length. The movement of the faults is strike-slip. Most of the authors concentrated on vertical faults. However, it is reported by many authors that the dip of the fault has an important role in the pattern of stress/strain accumulation near the fault. Here we have considered inclined faults with different inclinations to the free surface and have tried to obtain expressions for displacements, stresses and strains as a function of the dip of the fault. The faults are also buried i.e. they are situated at a depth from the free surface. The nature of stress- strain accumulation across one fault is affected by another fault. In this study, the effect of one fault movement on the other has been analysed during three situations which are (i) in the absence of fault movement, (ii) due to the movement of nonplanar fault only and (iii) due to the movement across both the faults. The effect of ground deformation on displacement and strain as well as the effect of movement of nonplanar fault on planar fault has been observed.

Table 1. Table for notation used in this study.

Name	Symbol Used	Description
Coordinates and Geometry	(y_1, y_2, y_3)	Cartesian coordinates with $y_3 = 0$ at the free surface, $y_3 > 0$ pointing downward
	$(y_1', y_2', y_3'), (y_1'', y_2'', y_3'')$	Coordinates associated with planar parts F_1 and F_2 of the nonplanar fault F
	$(z_1, z_2, z_3), (y_1''', y_2''', y_3''')$	Coordinates associated with finite fault F_3
	d_1, d_2, d_3	Depth of F_1, F_2, F_3 from the free surface
	D_1, D_2, D_3	Widths of F_1, F_2, F_3
	$2L$	Length of the finite fault F_3
	D	Horizontal distance between the faults F and F_3
	H	Thickness of the elastic layer
	$\theta_1, \theta_2, \theta_3$	Inclinations of F_1, F_2, F_3 relative to the free surface
Material Parameters	μ_1, μ_2	Rigidity (shear modulus) of elastic layer and viscoelastic half-space
	η	Viscosity of viscoelastic half-space
Displacements, Strains and Stresses	u_i, u_i'	Displacement components in layer and half-space ($i = 1, 2, 3$)
	τ_{ij}, τ_{ij}'	Stress components in layer and half-space
	e_{ij}, e_{ij}'	Strain components in layer and half-space
	T_{12}, T_{12}'	Shear stress at fault midpoints
Fault Creep	v_1, v_2, v_3	Creep velocities across F_1, F_2, F_3
	$U_1(t), V_1(t), U_2(t)$	Slip displacement functions across F_1, F_2, F_3
	$f_1(y_3'), f_2(y_3''), f_3(y_1''', y_3''')$	Spatial creep functions across F_1, F_2, F_3

2. Methodology

The movement of interacting faults in a layered composite structure comprised of an elastic layer of thickness H overlying a viscoelastic half-space of Maxwell medium has been considered (**Figure 1**). Two buried strike-slip faults F and F_3 are situated in elastic layer where F is infinite and F_3 is finite in length. The fault F is nonplanar consisting of two planar parts F_1 and F_2. The non planarity occur at the point O'' at a depth $(d_1 + d_2)$ from the free surface. The inclination with the free surface across F_1 is θ_1 and F_2 is θ_2. Let the width of F_1 and F_2 are D_1 and D_2 respectively. The depth from the free surface of F_1 and F_2 are d_1 and $(d_1 + d_2)$ respectively. Let $2L$ be the length of the finite fault F_3 and the co-ordinates of the end points of F_3 are $A(-L, 0, 0)$ and $B(L, 0, 0)$. θ_3 is the inclination of the fault F_3 with the horizon, D_3 is the width and d_3 is the depth of the fault F_3 from the free surface. The distance between F and F_3 on the free surface is represented by D.

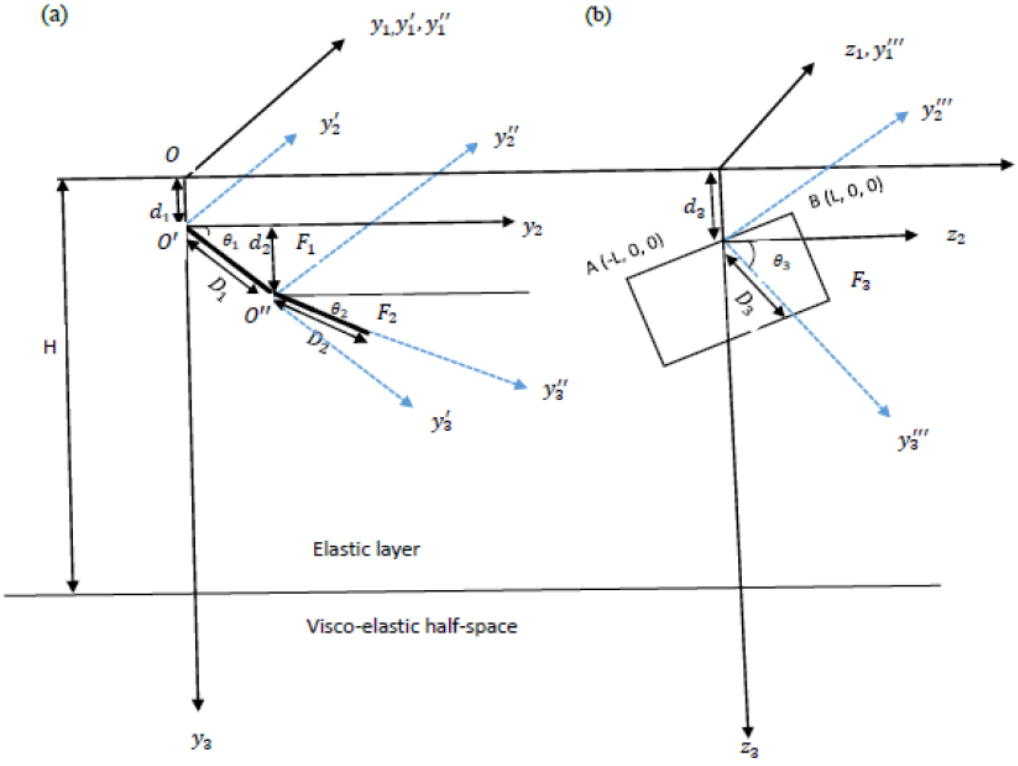

Figure 1. Fault model containing non-planar and planar fault.

The above parameters have direct seismological interpretations. The creep velocity functions adopted here represent steady aseismic slip commonly observed in interseismic and postseismic periods. The continuity of displacement and stress at the elastic-viscoelastic interface reflects the welded contact between lithosphere and asthenosphere, allowing stress transfer from brittle crust to ductile substrate. The burial depth of faults controls the amplitude of surface deformation, with shallow faults leading to stronger and more localized displacements. Similarly, dip angle affects strain distribution, with steeper dips concentrating deformation and shallower dips spreading it over a wider area. The finite widths of the faults correspond to seismogenic thickness, while the inter-fault distance regulates the degree of mechanical interaction and potential stress triggering between neighboring faults.

To represent the model, we introduce a rectangular cartesian co-ordinate system (y_1, y_2, y_3) with the plane free surface has been chosen for F as $y_3 = 0$ and y_3 axis pointing into the half-space. For the convenience of our mathematical computations, we have introduced two more rectangular cartesian co-ordinate systems (y_1', y_2', y_3') and (y_1'', y_2'', y_3'') associated with the planar parts F_1 and F_2 of the fault respectively with origin $O'(0, 0, d_1)$ and $O''(0, D_1 \cos\theta_1, D_1 \sin\theta_1 + d_1)$ respectively. The displacement, stress and strain components in the layer are taken as u_i, τ_{ij} and e_{ij} $(i, j = 1, 2, 3)$ respectively and in viscoelastic substrate are defines as u_i', τ_{ij}' and e_{ij}' $(i, j = 1, 2, 3)$ respectively.

The fault is represented by ($F_1 : y_2' = 0, 0 \leq y_3' \leq D_1$ and $F_2 : y_2'' = 0, 0 \leq y_3'' \leq D_2$).

The relation between (y_1, y_2, y_3), (y_1', y_2', y_3') and (y_1'', y_2'', y_3'') are given by:

$$y_1 = y_1'$$
$$y_2 = y_2' \sin\theta_1 + y_3' \cos\theta_1$$
$$y_3 = -y_2' \cos\theta_1 + y_3' \sin\theta_1 + d_1$$

and

$$y_1 = y_1''$$
$$y_2 = D_1 \cos\theta_1 + y_2'' \sin\theta_2 + y_3'' \cos\theta_2$$
$$y_3 = D_1 \sin\theta_1 - y_2'' \cos\theta_2 + y_3'' \sin\theta_2 + d_1$$

A segment of the theoretical model along the plane $y_1 = 0$ is illustrated in in **Figure 1** where the coordinate axes (y_2, y_3), (y_2', y_3') and (y_2'', y_3'') are also identified.

For the finite fault F_3 the rectangular cartesian co-

ordinate system has been considered as (z_1, z_2, z_3) and (y_1''', y_2''', y_3'''). z_3 axis pointing into the half-space with $z_3 = 0$ is the free surface. The co-ordinate system is associated by the following relation:

$$y_1''' = z_1$$
$$y_2''' = z_2 \sin\theta_3 - z_3 \cos\theta_3$$
$$y_3''' = z_2 \cos\theta_3 + z_3 \sin\theta_3$$

where $z_2 = y_2 - D$ and $z_3 = y_3 - d_1 - d_2$

The faults are given by

$$F : \big(F_1 :\ y_2' = 0,\ 0 \le y_3' \le D_1$$
$$F_2 :\ y_2'' = 0,\ 0 \le y_3'' \le D_2\big)$$
$$F_3 : \big(-L \le y_1''' \le L,\ y_2''' = 0,\ 0 \le y_3''' \le D_3\big)$$

2.1. Constitutive Equation

For a linear elastic layer, the constitutive law states that "Strain is proportional to stress suggested" by Ghosh et al.[22]. Consequently, the constitutive equations governing both the infinite and finite faults adhere to the following relationships:

across infinite fault F

$$\left.\begin{aligned} \tau_{12} &= \mu_1 \left(\tfrac{\partial u_1}{\partial y_2}\right) \\ \tau_{13} &= \mu_1 \left(\tfrac{\partial u_1}{\partial y_3}\right) \end{aligned}\right\} \tag{1}$$

across finite fault F_3

$$\tau_{ij} = \mu_1 \left(\frac{\partial u_i}{\partial y_j} + \frac{\partial u_j}{\partial y_i}\right), \text{where } i, j = 1, 2, 3 \quad (0 \le y_3 \le H,\ -\infty < y_2 < \infty,\ t \ge 0) \tag{2}$$

In the linear viscoelastic half-space of Maxwell medium across infinite fault F

$$\left.\begin{aligned} \left(\frac{1}{\eta} + \frac{1}{\mu_2}\frac{\partial}{\partial t}\right)\tau_{12}^{'} &= \frac{\partial}{\partial t}\left(\frac{\partial u_1^{'}}{\partial y_2} + \frac{\partial u_2^{'}}{\partial y_1}\right) \\ \left(\frac{1}{\eta} + \frac{1}{\mu_2}\frac{\partial}{\partial t}\right)\tau_{13}^{'} &= \frac{\partial}{\partial t}\left(\frac{\partial u_1^{'}}{\partial y_3} + \frac{\partial u_3^{'}}{\partial y_1}\right) \end{aligned}\right\} \tag{3}$$

across finite fault F_3

$$\left(\frac{1}{\eta} + \frac{1}{\mu_2}\frac{\partial}{\partial t}\right)\tau_{ij}^{'} = \frac{\partial}{\partial t}\left(\frac{\partial u_i^{'}}{\partial y_j} + \frac{\partial u_j^{'}}{\partial y_i}\right), (i, j = 1, 2, 3) \quad (y_3 > H,\ -\infty < y_2 < \infty,\ t \ge 0) \tag{4}$$

Here, t denotes time, μ_1, μ_2 represents the rigidities of the material of layer and substrate respectively and η represents the viscosity of the substrate.

2.2. Quasi-static Equilibrium Equation

The Quasi-static Equilibrium equation can be expressed as:

In the linear elastic layer

across infinite fault

$$\frac{\partial}{\partial y_2}(\tau_{12}) + \frac{\partial}{\partial y_3}(\tau_{13}) = 0 \tag{5}$$

across finite fault

$$\left.\begin{aligned} \frac{\partial}{\partial y_1}(\tau_{11}) + \frac{\partial}{\partial y_2}(\tau_{12}) + \frac{\partial}{\partial y_3}(\tau_{13}) &= 0 \\ \frac{\partial}{\partial y_1}(\tau_{21}) + \frac{\partial}{\partial y_2}(\tau_{22}) + \frac{\partial}{\partial y_3}(\tau_{23}) &= 0 \\ \frac{\partial}{\partial y_1}(\tau_{31}) + \frac{\partial}{\partial y_2}(\tau_{32}) + \frac{\partial}{\partial y_3}(\tau_{33}) &= 0 \end{aligned}\right\} \tag{6}$$

In Viscoelastic half-space

across infinite fault

$$\frac{\partial}{\partial y_2}(\tau_{12}') + \frac{\partial}{\partial y_3}(\tau_{13}') = 0 \tag{7}$$

across finite fault

$$\left.\begin{aligned} \frac{\partial}{\partial y_1}(\tau_{11}') + \frac{\partial}{\partial y_2}(\tau_{12}') + \frac{\partial}{\partial y_3}(\tau_{13}') &= 0 \\ \frac{\partial}{\partial y_1}(\tau_{21}') + \frac{\partial}{\partial y_2}(\tau_{22}') + \frac{\partial}{\partial y_3}(\tau_{23}') &= 0 \\ \frac{\partial}{\partial y_1}(\tau_{31}') + \frac{\partial}{\partial y_2}(\tau_{32}') + \frac{\partial}{\partial y_3}(\tau_{33}') &= 0 \end{aligned}\right\} \tag{8}$$

2.3. Initial and Boundary Conditions

The boundary conditions are specified at time $t = 0$, i.e. during the period when the medium is in an aseismic state. The fault F begins to move at time $t = T_1(> 0)$ followed by the finite fault F_3, which starts moving at time $t = T_2(> 0)$, where $T_1 < T_2$. The boundary condition is described in **Figure 2**, which is as follows:

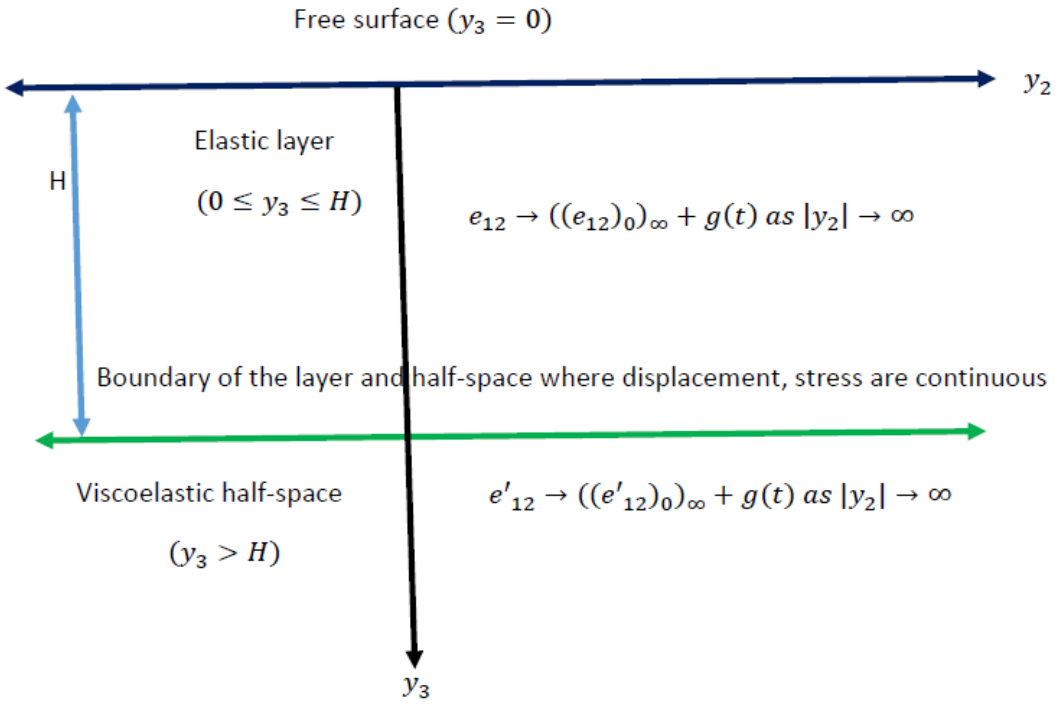

Figure 2. Geometrical representation of boundary conditions.

(a) Initial aseismic state (at $t = 0$)

- The medium is stress-free except for background tectonic loading.
- Displacements, stresses and strains satisfy

$$u_i = (u_i)_0, \tau_{ij} = (\tau_{ij})_0, e_{ij} = (e_{ij})_0 \quad \text{for } i, j = 1, 2, 3$$

- Far-field shear stress and strain evolve according to a continuous loading function $g(t)$, with $g(0) = 0$:

$$e_{12} \to (e_{12})_{0,\infty} + g(t),$$
$$e'_{12} \to (e'_{12})_{0,\infty} + g(t), |y_2| \to \infty$$

(b) Onset of fault creep

- The infinite nonplanar fault F begins to slip at time $t = T_1 > 0$
  The finite fault F_3 begins to slip later at $t = T_2 > T_1$
  Fault slips are modelled as creep with velocity-controlled displacement discontinuities:

$$[u_1]_F = U_1(t - T_1) f_1(y'_3) + V_1(t - T_1) f_2(y''_3), \quad t \ge T_1$$
$$[u_1]_{F_3} = U_2(t - T_2) f_3(y'''_1, y'''_3), \quad t \ge T_2$$

(c) Free surface condition

- At the Earth's surface ($y_3 = 0$), the traction vanishes:

$$\tau_{13} = 0$$

(d) Interface continuity

- At the welded contact ($y_3 = H$) between the elastic layer and viscoelastic half-space:

$$u_1 = u'_1 \text{ and } \tau_{13} = \tau'_{13}$$

(e) Far-field condition

- At great depths and far from the fault trace:
  $\tau_{13} \to 0$ as $y_3 \to \infty$ $(-\infty < y_2 < \infty, t \ge 0)$
  $e_{12} \to (e_{12})_{0,\infty} + g(t)$ for layer and $e'_{12} \to (e'_{12})_{0,\infty} + g(t)$ for half-space

where $(e_{12})_{0,\infty} = \lim_{|y_2|\to\infty}(e_{12})_0$
and $(e'_{12})_{0,\infty} = \lim_{|y_2|\to\infty}(e'_{12})_0$

(f) Symmetry condition

- As $|y_2| \to \infty$, fault-induced perturbations vanish and the field approaches the far-field loading state.

3. Solution

Differentiating the first and second equations of (1) with respect to y_2 and y_3, respectively, and then adding the results, while incorporating equation (5), yields the following (in the elastic layer):

$$\nabla^2 u_1 = 0 \quad \text{in} \quad 0 \le y_3 \le H \tag{9}$$

Or,

$$\nabla^2 \overline{u_1} = 0, \ \overline{u_1} \tag{10}$$

is the Laplace transform of u_1 with respect to time t.

Differentiate 1st equation of (3) with respect to y_2 and 2nd equation of (3) with respect to y_3. After that adding and finally using (7), we obtain (in viscoelastic half space), $\nabla^2 u_1' = c$, where c is a constant.

At, $t = 0$, $u_1' = (u_1')_0$, so $c = \nabla^2 (u_1')_0$

Then $\nabla^2 u_1' = \nabla^2 (u_1')_0$

Or, $\nabla^2 \left(u_1' - (u_1')_0\right) = 0$

Or,

$$\nabla^2 U_1' = 0 \quad \text{in} \quad y_3 \ge H \tag{11}$$

where $U_1^{'} = (u)_1^{'} - \left(u_1^{'}\right)_0$

Taking Laplace transform with respect to time t we find, $\nabla^2 \overline{U}_1' = 0$, $\overline{U}_1'$ is the Laplace transform of U_1' with respect to time t and

$$\overline{U}_1' = \overline{u}_1' - (\overline{u}_1')_0 \tag{12}$$

From equation (11) and (14) it is found that $\overline{u}_1$ and $\overline{u_1'}$ are linear solution, then let's assume that

$$\overline{u}_1 = \frac{(u_1)_0}{s} + A_1 y_2 + B_1 y_3 \tag{13}$$

and

$$\overline{u}_1' = \frac{(u_1')_0}{s} + A_2 y_2 + B_2 y_3 \tag{14}$$

3.1. Solution in the Absence Oo Any Fault Movement

Taking the Laplace transform on equations (1) to (8) with respect to time t, we obtain the exact solutions for displacements, stresses and strains which represent a boundary value problem. Then solving this boundary value problem, the value of constants A_1, B_1, A_2, B_2 are found.

Finally, the solutions are obtained by taking inverse Laplace transform for $t < T_1$ which are as follows:

For elastic layer

$$\left.\begin{aligned} u_1 &= (u_1)_0 + y_2 g(t) \\ \tau_{12} &= (\tau_{12})_0 + \mu_1 g(t) \\ \tau_{13} &= (\tau_{13})_0 \\ e_{12} &= (e_{12})_0 + g(t) \\ e_{13} &= (e_{13})_0 \end{aligned}\right\} \tag{15}$$

For half-space

$$\left.\begin{aligned} u_1' &= (u_1')_0 + y_2 g(t) \\ \tau_{12}' &= (\tau_{12}')_0 e^{-\frac{\mu_2}{\eta} t} + \mu_2 g(t) \\ \tau_{13}' &= (\tau_{13}')_0 e^{-\frac{\mu_2}{\eta} t} \\ e_{12}' &= (e_{12}')_0 + g(t) \\ e_{13}' &= (e_{13}')_0 \end{aligned}\right\} \tag{16}$$

Now the stress at the midpoint of the fault F is defined by T_{12} and

$T_{12} = \tau_{12} \sin\theta_1 - \tau_{13} \cos\theta_1 = (T_{12})_0 + \mu_1 g(t) \sin\theta_1$ where $(T_{12})_0 = (\tau_{12})_0 \sin\theta_1 - (\tau_{13})_0 \cos\theta_1$.

From the obtained solution, it is observed that $\tau_{13}'|_{\text{across } F} \to 0$ as $t \to \infty$ and $\tau_{12}'|_{\text{across} F}$ remains bounded. It is concluded that fault slip or the fault slip is more likely to occur in the layer above the substrate.

3.2. Solution after the Commencement of Non-Planar Fault Movement

The solution of displacement, stress and strain components due to the interaction between F and F_3 are in the following form:

in layer

$$\left.\begin{aligned} u_i &= (u_i)_1 + (u_i)_2 + (u_i)_3 + (u_i)_4 \\ \tau_{ij} &= (\tau_{ij})_1 + (\tau_{ij})_2 + (\tau_{ij})_3 + (\tau_{ij})_4 \\ e_{ij} &= (e_{ij})_1 + (e_{ij})_2 + (e_{ij})_3 + (e_{ij})_4 \end{aligned}\right\} \tag{17}$$

where $(u_i)_1, (\tau_{ij})_1, (e_{ij})_1$ are displacement, stress and strain components before the fault movement $t < T_1$. $(u_i)_2 + (u_i)_3, (\tau_{ij})_2 + (\tau_{ij})_3, (e_{ij})_2 + (e_{ij})_3$ are displacements, stresses and strains due to movement across non-planar fault F (for $t \geq T_1$), $(u_i)_4, (\tau_{ij})_4, (e_{ij})_4$ are displacement, stress and strain components due to movement across planar fault F_3 (for $t \geq T_2$).

Similarly, the solutions in the half-space are

$$\left.\begin{aligned} u_i' &= (u_i')_1 + (u_i')_2 + (u_i')_3 + (u_i')_4 \\ \tau_{ij}' &= (\tau_{ij}')_1 + (\tau_{ij}')_2 + (\tau_{ij}')_3 + (\tau_{ij}')_4 \\ e_{ij}' &= (e_{ij}')_1 + (e_{ij}')_2 + (e_{ij}')_3 + (e_{ij}')_4 \end{aligned}\right\} \quad (18)$$

where $(u_i')_1, (\tau_{ij}')_1, (e_{ij}')_1$ are displacement, stress and strain components before the fault movement $(t < T_1)$, $(u_i')_2 + (u_i')_3, (\tau_{ij}')_2 + (\tau_{ij}')_3, (e_{ij}')_2 + (e_{ij}')_3$ are due to movement across the non-planar fault F (for $t \geq T_1$) while $(u_i)_4, (\tau_{ij})_4, (e_{ij})_4$ are due to movement across planar fault F_3 (for $t \geq T_2$). Now $(u_1)_2$, $(\tau_{12})_2$, $(\tau_{13})_2$, $(e_{12})_2$, $(u_1)_3$, $(\tau_{12})_3$, $(\tau_{13})_3$, $(e_{12})_3$, $(u_1')_2$, $(\tau_{12}')_2$, $(\tau_{13}')_2$, $(e_{12}')_2$, $(u_1')_3$, $(\tau_{12}')_3$, $(\tau_{13}')_3$, $(e_{12}')_3$ are assumed to be zero for $t < T_1$ and satisfy constitutive equation, stresses equation of motion and boundary conditions with the modified strain condition $(e_{12}) \to 0$ and $(e_{12}') \to 0$ for $t_1 (= t - T_1) \geq 0$ and $|y_2| \to \infty$, $|y_2'| \to \infty$. The displacement, stresses, and strains are continuous throughout the model, except across the fault F, where the displacement component exhibits a discontinuity. The condition that characterizes the creeping movement across the fault F is

$[u_1]_F = U_1(t_1) f_1(y_3') H(t_1) + V_1(t_1) f_2(y_3'') H(t_1)$, where $y_2' = 0,\ 0 \leq y_3' \leq D_1$ and $y_2'' = 0,\ 0 \leq y_3'' \leq D_2$ where $t_1 = t - T_1$, $f_1(y_3')$ and $f_2(y_3'')$ represent the spatial dependence of the creep movement along the widths of F_1 and F_2 respectively, $H(t_1)$ is Heaviside unit step function. So

$$[u_1]_F = U_1(t_1) f_1(y_3') H(t_1) + V_1(t_1) f_2(y_3'') H(t_1) = \begin{cases} 0 & \text{for } t_1 \leq 0 \\ U_1(t_1) f_1(y_3') + V_1(t_1) f_2(y_3'') & \text{for } t_1 > 0 \end{cases} \quad (19)$$

and for calculating displacement after the fault movement, we have taken $t > T_1$ i.e $t_1 > 0$ (T_1 is the time when the fault F starts to move) then

$$[u_1]_F = U_1(t_1) f_1(y_3') + V_1(t_1) f_2(y_3'') \quad (20)$$

The discontinuity of u_1 across F is given by

$$[u_1]_F = \log_{\left(y_1', y_2''\right) \to (0^+, 0^+)} u_1 - \log_{\left(y_1', y_2''\right) \to (0^-, 0^-)} u_1 \quad (21)$$

Here $U_1(t_1)$, $V_1(t_1)$ are continuous function of y_3' and y_3'' respectively. $U_1(t_1) = 0$, $V_1(t_1) = 0$ for $t_1 < 0$ and $U_1(t_1) = v_1 t_1$, $V_1(t_1) = v_2 t_1$ for $t_1 \geq 0$, where v_1 and v_2 are creep velocity across two non-planar parts F_1 and F_2 of F. Now Laplace transform of equation (20) with respect to t_1 gives $[\overline{u_1}]_F = \overline{U_1}(s) f_1(y_3') + \overline{V_1}(s) f_2(y_3'')$, where $U_1(s)$ and $V_1(s)$ are Laplace transform of $U_1(t_1)$ and $V_1(t_1)$, s is Laplace transform variable.

By using Laplace transform, inverse Laplace transform and Green's function method (details given in **APPENDIX A** for layer and **APPENDIX B** for half-space) the displacements, stresses and strains across the non-planar fault is obtained as follows:

For layer

$$\left.\begin{aligned} (u_1)_2 + (u_1)_3 &= H(t_1) \frac{U_1(t_1)}{2\pi} \phi + H(t_1) \frac{V_1(t_1)}{2\pi} \psi \\ (\tau_{12})_2 + (\tau_{12})_3 &= \mu_1 H(t_1) \frac{U_1(t_1)}{2\pi} \phi_2 + \mu_1 H(t_1) \frac{V_1(t_1)}{2\pi} \psi_2 \\ (\tau_{13})_2 + (\tau_{13})_3 &= \mu_1 H(t_1) \frac{U_1(t_1)}{2\pi} \phi_3 + \mu_1 H(t_1) \frac{V_1(t_1)}{2\pi} \psi_3 \\ (e_{12})_2 + (e_{12})_3 &= H(t_1) \frac{U_1(t_1)}{2\pi} \phi_2 + H(t_1) \frac{V_1(t_1)}{2\pi} \psi_2 \\ (e_{13})_2 + (e_{13})_3 &= H(t_1) \frac{U_1(t_1)}{2\pi} \phi_3 + H(t_1) \frac{V_1(t_1)}{2\pi} \psi_3 \end{aligned}\right\} \quad (22)$$

where the expressions of ϕ and ψ are given in **APPENDIX A** and $\phi_2 = \frac{\partial \phi}{\partial y_2}$, $\phi_3 = \frac{\partial \phi}{\partial y_3}$, $\psi_2 = \frac{\partial \psi}{\partial y_2}$, $\psi_3 = \frac{\partial \psi}{\partial y_3}$.

For half-space

$$\left.\begin{aligned} (u_1')_2 + (u_1')_3 &= H(t_1) \frac{U_1(t_1)}{2\pi} \phi' + H(t_1) \frac{V_1(t_1)}{2\pi} \psi' \\ (\tau_{12}')_2 + (\tau_{12}')_3 &= \mu_2 H(t_1) \frac{U_1(t_1)}{2\pi} \phi_2' + \mu_2 H(t_1) \frac{V_1(t_1)}{2\pi} \psi_2' \\ (\tau_{13}')_2 + (\tau_{13}')_3 &= \mu_2 H(t_1) \frac{U_1(t_1)}{2\pi} \phi_3' + \mu_2 H(t_1) \frac{V_1(t_1)}{2\pi} \psi_3' \\ (e_{12}')_2 + (e_{12}')_3 &= H(t_1) \frac{U_1(t_1)}{2\pi} \phi_2' + H(t_1) \frac{V_1(t_1)}{2\pi} \psi_2' \\ (e_{13}')_2 + (e_{13}')_3 &= H(t_1) \frac{U_1(t_1)}{2\pi} \phi_3' + H(t_1) \frac{V_1(t_1)}{2\pi} \psi_3' \end{aligned}\right\} \quad (23)$$

where the expressions of ϕ' and ψ' are given in **APPENDIX B** and $\phi_2' = \frac{\partial \phi'}{\partial y_2}$, $\phi_3' = \frac{\partial \phi'}{\partial y_3}$, $\psi_2' = \frac{\partial \psi'}{\partial y_2}$, $\psi_3' = \frac{\partial \psi'}{\partial y_3}$.

3.3. Solution after the Commencement of the Planar Fault Movement

After time T_2 ($T_2 > T_1$), i.e after commencement of creeping movement across F, there is a movement across the planar fault F_3 when the accumulated stress near it exceeds the critical value τ_{c_2}. The slip condition across F_3 is characterized by

$$[u_1]_{F_3} = U_2(t_2) f_3(y_1''', y_3''') H(t_2), (-L \le y_1''' \le L, \; y_2''' = 0, \; 0 \le y_3''' \le D_3, \; t_2 > 0, \; t_2 = t - T_2) \tag{24}$$

Here $H(t_2)$ is the Heaviside function, $f_3(y_1''', y_3''')$ gives the spatial dependence of the slip movement along the fault F_3 and $U_2(t_2) = v_3 t_2$, v_3 is creep velocity of the fault movement across F_3.

$$[u_1]_{F_3} = U_2(t_2) f_3(y_1''', y_3''') H(t_2) = \begin{cases} 0, & \text{for } t_2 \le 0 \\ U_2(t_2) f_3(y_1''', y_3'''), & \text{for } t_2 > 0 \end{cases}$$

Since the fault F_3 starts to move at $t > T_2$ that is $t_2 > 0$ then

$$[u_1]_{F_3} = U_2(t_2) f_3(y_1''', y_3''') H(t_2) \tag{25}$$

The discontinuity of the displacement component u_1 across F_3 is given by

$$[u_1]_{F_3} = \lim_{y_2''' \to 0^+} u_1 - \lim_{y_2''' \to 0^-} u_1 \tag{26}$$

Taking Laplace transform of equation (25) with respect to t_2 we obtain $[\overline{u_1}]_{F_3} = \overline{U_2}(s) f_3(y_1''', y_3''')$, where $\overline{U_2}(s)$ is the Laplace transform of $U_2(t_2)$.

The boundary value problem (BVP) thus obtained can be addressed using the modified Green's function method (details given in **Appendix A** for layer and **Appendix B** for half-space). The solution of the BVP across F_3 for $t \ge T_2$ are as follows:

For layer

$$\left.\begin{aligned} (u_1)_4 &= \frac{U_2(t_2)}{2\pi} \chi(z_1, z_2, z_3) H(t_2) \\ (u_2)_4 &= 0 \\ (u_3)_4 &= 0 \\ (\tau_{11})_4 &= \mu_1 H(t_2) \frac{U_2(t_2)}{\pi} \chi_1 \\ (\tau_{12})_4 &= \mu_1 H(t_2) \frac{U_2(t_2)}{2\pi} \chi_2 \\ (\tau_{13})_4 &= \mu_1 H(t_2) \frac{U_2(t_2)}{2\pi} \chi_3 \\ (\tau_{23})_4 &= 0 \\ (\tau_{22})_4 &= 0 \\ (\tau_{33})_4 &= 0 \\ (e_{12})_4 &= H(t_2) \frac{U_2(t_2)}{4\pi} \chi_2 \\ (e_{13})_4 &= H(t_2) \frac{U_2(t_2)}{4\pi} \chi_3 \end{aligned}\right\} \tag{27}$$

For half-space

$$\begin{aligned} (u_1')_4 &= \tfrac{U_2(t_2)}{2\pi} \chi'(z_1, z_2, z_3) H(t_2) \\ (u_2')_4 &= 0 \\ (u_3')_4 &= 0 \\ (\tau_{11}')_4 &= \mu_2 \tfrac{H(t_2)}{\pi} \left[U_2(t_2) - \tfrac{\mu_2}{\eta} \int_0^{t_2} U_2(\tau) e^{-\frac{\mu_2}{\eta}(t_2 - \tau)} d\tau \right] \chi_1' \\ (\tau_{12}')_4 &= \mu_2 \tfrac{H(t_2)}{2\pi} \left[U_2(t_2) - \tfrac{\mu_2}{\eta} \int_0^{t_2} U_2(\tau) e^{-\frac{\mu_2}{\eta}(t_2 - \tau)} d\tau \right] \chi_2' \\ (\tau_{13}')_4 &= \mu_2 \tfrac{H(t_2)}{2\pi} \left[U_2(t_2) - \tfrac{\mu_2}{\eta} \int_0^{t_2} U_2(\tau) e^{-\frac{\mu_2}{\eta}(t_2 - \tau)} d\tau \right] \chi_3' \\ (\tau_{23}')_4 &= e^{-\frac{\mu_2}{\eta} t_2} (\tau_{23}')_0 \\ (\tau_{22}')_4 &= e^{-\frac{\mu_2}{\eta} t_2} (\tau_{22}')_0 \\ (\tau_{33}')_4 &= e^{-\frac{\mu_2}{\eta} t_2} (\tau_{33}')_0 \\ (e_{12}')_4 &= H(t_2) \tfrac{U_2(t_2)}{4\pi} \chi_2' \\ (e_{13}')_4 &= H(t_2) \tfrac{U_2(t_2)}{4\pi} \chi_3' \end{aligned} \tag{28}$$

where the expressions of χ and χ' are given in **APPENDIX A** and **APPENDIX B** respectively and $\chi_2 = \frac{\partial \chi}{\partial y_2}$, $\chi_3 = \frac{\partial \chi}{\partial y_3}$, $\chi_2' = \frac{\partial \chi'}{\partial y_2}$, $\chi_3' = \frac{\partial \chi'}{\partial y_3}$.

Now the final solution of displacements, stresses and strains after the interaction between infinite non-planar strike-slip fault F and finite planar strike-slip fault F_3 can be obtained as follows:

In elastic layer

$$\left.\begin{aligned}
u_1 &= (u_1)_0 + y_2 g(t) + H(t_1)\frac{U_1(t_1)}{2\pi}\phi + H(t_1)\frac{V_1(t_1)}{2\pi}\psi + \frac{U_2(t_2)}{2\pi}\chi(z_1,z_2,z_3)H(t_2)\\
u_2 &= 0\\
u_3 &= 0\\
\tau_{11} &= \mu_1 H(t_2)\frac{U_2(t_2)}{\pi}\chi_1\\
\tau_{12} &= (\tau_{12})_0 + \mu_1 g(t) + \mu_1 H(t_1)\frac{U_1(t_1)}{2\pi}\phi_2 + \mu_1 H(t_1)\frac{V_1(t_1)}{2\pi}\psi_2 + \mu_1 H(t_2)\frac{U_2(t_2)}{2\pi}\chi_2\\
\tau_{13} &= (\tau_{13})_0 + \mu_1 H(t_1)\frac{U_1(t_1)}{2\pi}\phi_3 + \mu_1 H(t_1)\frac{V_1(t_1)}{2\pi}\psi_3 + \mu_1 H(t_2)\frac{U_2(t_2)}{2\pi}\chi_3\\
\tau_{23} &= 0\\
\tau_{22} &= 0\\
\tau_{33} &= 0\\
e_{12} &= (e_{12})_0 + g(t) + H(t_1)\frac{U_1(t_1)}{4\pi}\phi_2 + H(t_1)\frac{V_1(t_1)}{4\pi}\psi_2 + H(t_2)\frac{U_2(t_2)}{4\pi}\chi_2\\
e_{13} &= (e_{13})_0 + H(t_1)\frac{U_1(t_1)}{4\pi}\phi_3 + H(t_1)\frac{V_1(t_1)}{4\pi}\psi_3 + H(t_2)\frac{U_2(t_2)}{4\pi}\chi_3
\end{aligned}\right\} \quad (29)$$

Shear stress at the midpoint of F and F_3 are respectively,

$(T'_{12})_{F\ (MID)} = (\tau_{12}\sin\theta_1 - \tau_{13}\cos\theta_1) + (\tau_{12}\sin\theta_2 - \tau_{13}\cos\theta_2) = (T'_{12})_{0F(MID)} + \mu_1 g(t)(\sin\theta_1 + \sin\theta_2) + \mu_1 H(t_1)\frac{U_1(t_1)}{2\pi}(\phi_2\sin\theta_1 - \phi_3\cos\theta_1 + \phi_2\sin\theta_2 - \phi_3\cos\theta_2) + \mu_1 H(t_1)\frac{V_1(t_1)}{2\pi}(\psi_2\sin\theta_1 - \psi_3\cos\theta_1 + \psi_2\sin\theta_2 - \psi_3\cos\theta_2) + \mu_1 H(t_2)\frac{U_2(t_2)}{2\pi}(\chi_2\sin\theta_1 - \chi_3\cos\theta_1 + \chi_2\sin\theta_2 - \chi_3\cos\theta_2)$

where $(T'_{12})_{0F(MID)} = (\tau_{12})_0(\sin\theta_1 + \sin\theta_2) - (\tau_{13})_0(\cos\theta_1 + \cos\theta_2)$

and

$(T'''_{12})_{F_3\ (MID)} = (\tau_{12}\sin\theta_3 - \tau_{13}\cos\theta_3) = (T'''_{12})_{0F_3(MID)} + \mu_1 g(t)\sin\theta_3 + \mu_1 H(t_1)\frac{U_1(t_1)}{2\pi}(\phi_2\sin\theta_3 - \phi_3\cos\theta_3) + \mu_1 H(t_1)\frac{V_1(t_1)}{2\pi}(\psi_2\sin\theta_3 - \psi_3\cos\theta_3) + \mu_1 H(t_2)\frac{U_2(t_2)}{2\pi}(\chi_2\sin\theta_3 - \chi_3\cos\theta_3)$

where $\left(T'''_{12}\right)_{0F(MID)} = (\tau_{12})_0\sin\theta_3 - (\tau_{13})_0$

In half-space

$$\left.\begin{aligned}
u'_1 &= (u_1)_0 + y_2 g(t) + H(t_1)\frac{U_1(t_1)}{2\pi}\phi' + H(t_1)\frac{V_1(t_1)}{2\pi}\psi' + \frac{U_2(t_2)}{2\pi}\chi'(z_1,z_2,z_3)H(t_2)\\
u'_2 &= 0\\
u'_3 &= 0\\
\tau'_{11} &= \mu_2\frac{H(t_2)}{2\pi}\left[U_2(t_2) - \frac{\mu_2}{\eta}\int_0^{t_2} U_2(\tau)e^{-\frac{\mu}{\eta}(t_2-\tau)}d\tau\right]\chi'_1\\
\tau'_{12} &= (\tau'_{12})_0 e^{-\frac{\mu}{\eta}t} + \mu_2 g(t) + \mu_1 H(t_1)\frac{U_1(t_1)}{2\pi}\phi'_2 + \mu_1 H(t_1)\frac{V_1(t_1)}{2\pi}\psi'_2 + \mu_2\frac{H(t_2)}{\pi}\left[U_2(t_2) - \frac{\mu}{\eta}\int_0^{t_2} U_2(\tau)e^{-\frac{\mu}{\eta}(t_2-\tau)}d\tau\right]\chi'_2\\
\tau'_{13} &= (\tau'_{13})_0 e^{-\frac{\mu}{\eta}t} + \mu_1 H(t_1)\frac{U_1(t_1)}{2\pi}\phi'_3 + \mu_1 H(t_1)\frac{V_1(t_1)}{2\pi}\psi'_3 + \mu_2\frac{H(t_2)}{\pi}\left[U_2(t_2) - \frac{\mu}{\eta}\int_0^{t_2} U_2(\tau)e^{-\frac{\mu}{\eta}(t_2-\tau)}d\tau\right]\chi'_3\\
\tau'_{23} &= e^{-\frac{\mu}{\eta}t_2}(\tau'_{23})_0\\
\tau'_{22} &= e^{-\frac{\mu}{\eta}t_2}(\tau'_{22})_0\\
\tau'_{33} &= e^{-\frac{\mu}{\eta}t_2}(\tau'_{33})_0\\
e'_{12} &= (e'_{12})_0 + g(t) + H(t_1)\frac{U_1(t_1)}{4\pi}\phi'_2 + H(t_1)\frac{V_1(t_1)}{4\pi}\psi'_2 + H(t_2)\frac{U_2(t_2)}{4\pi}\chi'_2\\
e'_{13} &= (e'_{13})_0 + H(t_1)\frac{U_1(t_1)}{4\pi}\phi'_3 + H(t_1)\frac{V_1(t_1)}{4\pi}\psi'_3 + H(t_2)\frac{U_2(t_2)}{4\pi}\chi_3
\end{aligned}\right\} \quad (30)$$

4. Numerical Results and Discussions

To recognize the behaviour of surface displacement, accumulation and release of stress-strain caused by the fault movement, their analytical solutions are analysed and the graphical representations are depicted using suitable values of model parameters (Cathles[23], Aki and Richards[24] and Clift et al.[25] and Karate[26]) which are given in **Table 2**.

Table 2. Parametric values.

Parameters	Symbol Used	Value Taken
Rigidity	μ_1	$3 \times 10^{10} N/m^2(Pascal)$
Rigidity	μ_2	$3.5 \times 10^{10} N/m^2(Pascal)$
Viscosity	η	$3 \times 10^{19}\ Pascal - s$
Width	D_1, D_2, D_3	5 km
Depth from the free surface	d_1, d_2, d_3	5 km, 4 km, 12 km
Distance between F and F_3 Horizontal distance of O″from O	D	8 km
Length of F_3	OO''	3 km
Thickness of the elastic layer	$2L$	20 km
Total time	H	10 km
Time of movement of non-planar fault F	t	200 year
Time of movement of planar fault F_3	T_1	50 year
Initial stress	T_2	100 year
Initial strain	$(\tau_{12})_0\,, (\tau_{13})_0$	$20 \times 10^5 N/m^2(Pascal)$
Stress for far away from the fault at time t	$(e_{12})_0\,, (e_{13})_0$	$20 \times 10^5 N/m^2(Pascal)$
Stress for far away from the fault at time 0	$\tau_\infty(t)$	$2 \times 10^7 N/m^2(Pascal)$
Constant	$\tau_\infty(0)$	$20 \times 10^5 N/m^2(Pascal)$
Inclination	k	10^{-9}
Creep velocity	$\theta_1, \theta_2, \theta_3$	$30^\circ, 45^\circ, 60^\circ, 90^\circ$
	v_1, v_2, v_3	0.01, 0.02, 0.03, 0.04 meter/yr

The value $of\tau_\infty$ is specified as 300 bars, aligning with the majority of estimations reported in similar research contexts (e.g., Sen, S. et al.[10]). The threshold level of shear stress τ_c,which represents the maximum shear stress that can be sustained by the frictional and cohesive forces acting across a fault, is influenced by the fault's inclination angle. For example, consider the upper segment F_1 of a fault F, where F_1 is inclined at an angle θ_1. Let us assume $\tau_c \approx \frac{1}{2}\tau_\infty \sin\theta_1$ for $F_1$and $\tau_\infty \sin\theta_1$ is the maximum value of shear stress $\left(T_{12}^{'}\right)_{F_1(MID)}$.Under the influence of the far-field shear stress τ_∞, the maximum shear stress that can accumulate near the fault segment F_1 is influenced by the inclination θ_1.The assumption introduces a stress-drop mechanism that occurs during creeping movement across the fault segment F_1. During a creeping event, two-thirds of the threshold shear stress ($\frac{2}{3}\tau_c$) is released and after the creeping movement stops and the system returns to an aseismic state, one-third of τ_c remains as residual stress when aseismic state re-established, so that at $t = 0$, $\left(T_{12}^{'}\right)_{0F_1(MID)} \approx \frac{1}{6}\tau_\infty \sin\theta_1$. It is observed that the stress near F_1under the influence of the far-field shear stress τ_∞takes approximately 50 years to accumulate to the threshold shear stress, so that $T_1 = 50$ years.

Creep function across nonplanar fault F:

for F_1 part $f_1(y_3') = R_1\left(1 - \frac{3y_3'^2}{D_1^2} + \frac{2y_3'^3}{D_4^3}\right)$ **(Figure 3)**

for F_2 part $f_2(y_3'') = \frac{R_2(y_3''^2 - D_2^2)}{(2D_2^4)}$ **(Figure 3)**

Creep function across planar fault F_3:

$f_1\left(y_1''',\ y_3'''\right) = R_3\left(1 - \frac{1}{L^2 y_1'''^2}\right)\left(1 - \frac{3y_3'^2}{D_3^2} + \frac{2y_3'^3}{D_3^3}\right)$ **(Figure 4)**

where $R_1,\ R_2$ and R_3 are constant and taken as 3m.

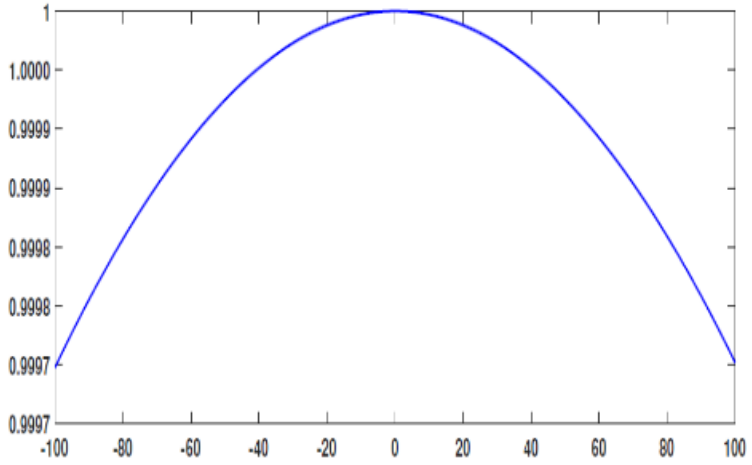

Figure 3. Creep function across infinite fault.

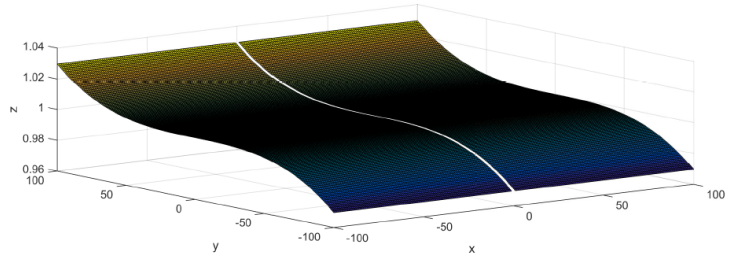

Figure 4. Creep function across the finite fault.

4.1. Effect of Nonplanarity on Rate of Displacement

The effect of nonplanarity on the rate of change of displacement against y_2 has been depicted through **Figure 5**. The rate of displacement is given by $R_{D_1} = \frac{\partial}{\partial t}\left[\frac{U_1(t_1)}{2\pi}H(t_1)\phi + \frac{V_1(t_1)}{2\pi}H(t_1)\psi + \frac{U_2(t_2)}{2\pi}H(t_2)\chi\right]$. Since the fault F is nonplanar and the nonplanarity occurs at the point O'' (at 3 km horizontal distance from the origin O) then R_D has been examined for distinct values of θ_2 in **Figure 5a**, where θ_2 is the inclined angle across F_2 with the free surface. It is observed that at a 3 km of horizontal distance from the origin O, the rate of change of displacement attains a minimum value for $\theta_2 = 90°$ and maximum value for $\theta_2 = 60°$. From this figure, it is concluded that if the inclination at the nonplanarity point is increasing from $60°$ towards $90°$ then the displacement due to interaction between planar and nonplanar fault is decreasing. From this figure, it is also observed that at a horizontal distance 8 km from the origin where the interaction occur the displacement rate attains maximum value at $\theta_2 = 30°$ and it decreases with increasing values of θ_2. The observation that there is a difference between the curves for $y_2 < 0$ with $y_2 > 0$. Since the interaction between nonplanar and planar faults occurs in the region where $y_2 > 0$ and this interaction leads to a variation in the rate of displacement in this region. R_D attains maximum value across the first planar part (F_1) of the nonplanar fault F. Then it decreases with increasing value of y_2. At the point O'' where F_1 interconnects with F_2, the rate of displacement increases slowly and when F fault interacts with F_3 then for $\theta_2 = 30°, 45°, 60°$, rate of displacement increases and after accomplishing a few values it diminishes towards zero. But if the structure of the fault is such as the nonplanar part F_2 is vertical with free surface, then after attaining maximum value at $y_2 = 0$, the displacement rate reduces towards zero. **Figure 5b** represent the displacement rate against the distance y_2 from the fault trace for distinct values of velocity of the fault movement has been established in **Figure 5b**. The observation that the rate of displacement increases with expanding values of velocity. The rate of displacement near the origin i.e. across F_1 attains maximum value and after that, it decreases for $y_2 \to 0^+$. At the point O'', where the nonplanarity occurs, the rate of displacement starts to increase slowly. When it interacts with the fault F_3, the rate of displacement increases rapidly, and after reaching a positive value, it decreases towards zero.

The effect of the depth of the faults on the rate of displacement has been established in **Figure 5c**. From this figure, it is concluded that rate of displacement increases with increasing value of depth across nonplanar fault. But when it starts to interact with planar fault then the rate of displacement attains maximum value for lower depth.

Comparing these figures with **Figure 5a** and **Figure 5b** of Karato[26], it shows that if both the interacting faults are planar then the displacement rate increases with increasing value of y_2 but if one nonplanar and other planer then the rate of displacement after attaining maximum value in first decreases and then increases and after that again decreases towards zero.

4.2. Effect of Nonplanarity on Rate of Change of Strain

Figure 6 illustrates the nature of change of surface shear strain (e_{12}) accumulation or releases due to fault movement across nonplanar fault. The rate of shear strain across the movement of F only (i.e there is no movement across (F_3) is $R_{s_1} = \frac{\partial}{\partial t}\left[\frac{U_1(t_1)}{4\pi}H(t_1)\phi_2 + \frac{V_1(t_1)}{4\pi}H(t_1)\psi_2\right]$. The variation of rate of shear strain against y_2 for different inclinations at the point O'' where nonplanarity has been depicted in **Figure 6a**. It is examined that the surface shear strain is accumulated steadily over time in the absence of any fault

movement. This strain accumulates its maximum value near $y_2 = 0$. But the curve near $y_2 = 0$ does not smoothly attain its maximum value which indicates the nonplanarity of F. Savage and Burford[27] have described the rate of accumulation as being of the order of 10^{-6} to 10^{-7} per year which is consistent with the observed rate of surface shear strain accumulation near the locked part of San Andreas fault in California. Here the shear strain accumulates its maximum value 5×10^{-7} (approximately) per year at $\theta_1 = 60°$ and $\theta_2 = 30°$. After fault movement starts, the strain accumulation rate diminishes, with the most significant drop near the fault. After reaching its peak value, it declines sharply, and once all the shear strain is released, it starts accumulating again toward zero.

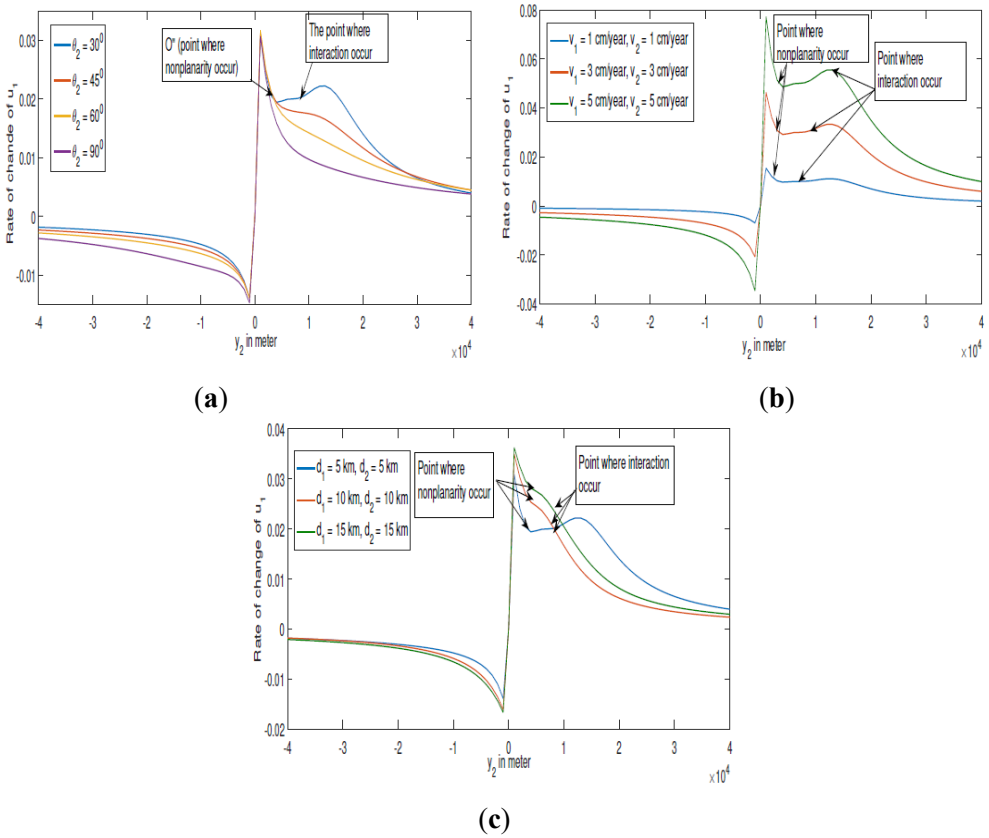

Figure 5. R_D against y_2 for different values. (**a**) θ_2; (**b**) velocity of the fault movement of the nonplanar fault; (**c**) depth of the nonplanar fault from the free surface.

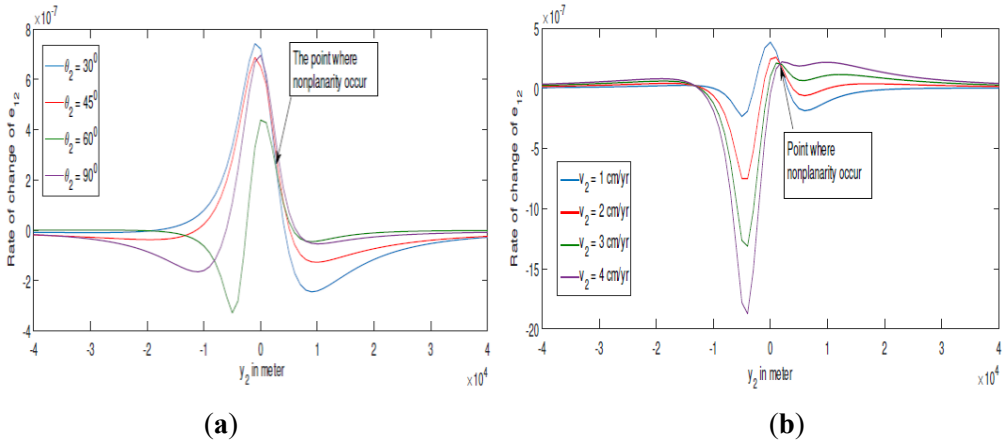

Figure 6. R_{s_1} against y_2 due to fault creep across F (no movement across F_3). (**a**) for different θ_1 when $\theta_2 = 60°$; (**b**) for different θ_2 when $\theta_1 = 60°$.

The effect of velocity (v_2) of the movement of nonplanar part F_2 when there is no movement across F_3 on the rate of shear strain against y_2 has been described in **Figure 6b**. It is analysed that for different creep velocity v_2 across F_2, R_{s_1} releases for $y_2 \to 0^-$. After releasing all the strain, it increases rapidly and near $y_2 \to 0^+$, it accumulates its maximum value. The amount of strain accumulation increases with decreasing value of velocity across the first planar part F_1 of the fault F. At the position O'' where nonplanarity occurs, the rate of shear strain releases and its value increases with increasing value of velocity.

The rate of change of shear strain due to interaction between F and F_3 is $R_{s_2} = \frac{\partial}{\partial t}\left[H(t_1)\frac{U_1(t_1)}{4\pi}\phi_2 + H(t_1)\frac{V_1(t_1)}{4\pi}\psi_2 + H(t_2)\frac{U_2(t_2)}{4\pi}\chi_2\right]$. The variation of R_{s_2} due to interaction between F and F_3 has been plotted in **Figure 7**. **Figure 7a** and **Figure 7b** delineates the accumulation or release of shear strain rate for distinct values of θ_1 and θ_2 when θ_3 is taken as $60°$. Near the fault F, R_{s_2} increases for all θ_1 and these increments in the value of R_{s_2} depend significantly on θ_3. As we move away from the fault F and approach fault F_3, R_{s_2} decreases first up to a certain level and then starts to increase as we gradually approach towards F_3 and reach an extreme value near F_3 as $y_2 \to D^+$. When θ_2 and θ_3 fixed then higher values of θ_1, higher the values of R_{s_1} near F_3. When θ_1 and θ_3 are fixed, the effect of inclination θ_2 on the rate of shear strain has been described in **Figure 7b**. It is found that after the accumulation of maximum shear strain across F, it falls off and after releasing a certain level it starts to increase when the movement occurs across F_3 at $y_2 = D$. After attaining a certain value, it again decreases towards zero for $y_2 > D$. Near F_3 rate of shear strain accumulation is maximum for $\theta_2 = 60°$ and minimum for $\theta_2 = 30°$ when θ_1 and θ_3 are taken as $45°$ and $60°$. It is observed that for $y_2 < 0$ there is no significant effect of inclinations on R_{s_2} across F_3. The strain accumulation curve at $y_2 = 0$ is not smooth which indicates the nonplanarity of the infinite fault F. Whereas near $y_2 = D$, the curve is smooth which indicates the planarity of the finite fault F_3. It is also illustrated that the accumulation rate of shear strain is more across F than F_3 which indicate that when a fault interacts with other then the amount of release of energy is greater across the first fault than the second fault that is the loss of life or properties is more affected near the first fault than the second fault.

The effect of creep velocity v_3 across F_3 has been described in **Figure 7c** when the creep velocity across F is fixed. It is observed that the shear strain accumulates maximum value across the fault F_3 i.e for $y_2 > D$ and it increases with increasing value of v_3. For $y_2 > D$, it falls off rapidly and gradually tends towards zero. If $\theta_1 = 30°$, $\theta_2 = 45°$, $\theta_3 = 60°$, $v_1 = 1\frac{cm}{year}$ and $v_2 = 1\frac{cm}{year}$, the shear strain accumulation rate across F is greater than F_3 when v_3 is 1 cm/year and 2cm/year but for $v_3 \geq 3$ cm/year, this accumulation rate is greater across F_3 than F. This indicates that for increasing velocity across F_3 the life or properties are more risk near the second fault than the first fault. **Figure 7d** depicts the effect of distance between F and F_3 on the rate of shear strain. It is noted that as the distance between F and F_3 increases, the location of shear strain accumulation across F_3 shifts further.

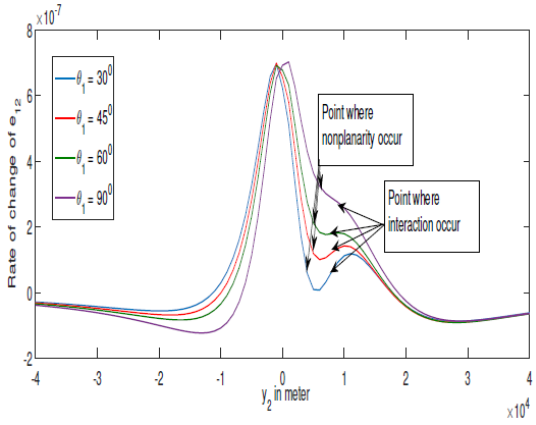

(a)

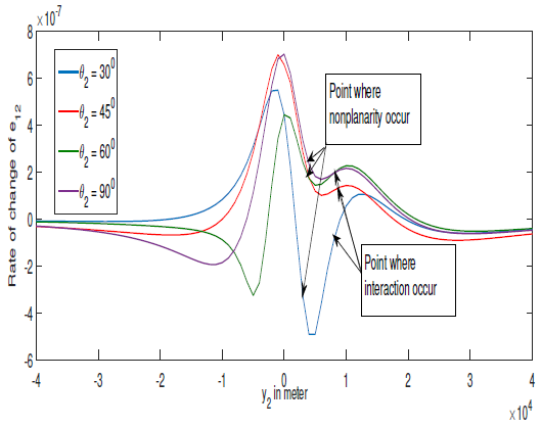

(b)

Figure 7. *Cont.*

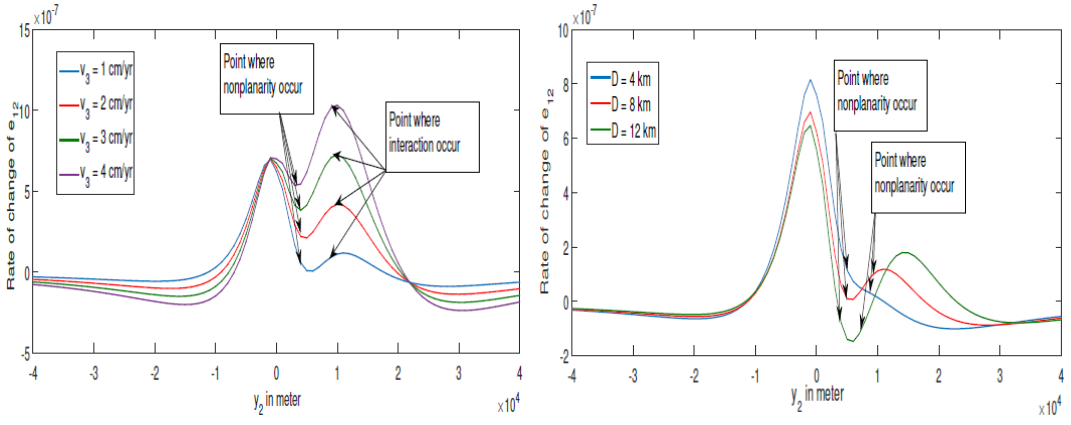

(c) **(d)**

Figure 7. Rate of change of surface shear strain (e_{12}) with y_2 due to interaction between F and F_3 . (**a**) for different θ_1 when $\theta_2 = 45^\circ$ and $\theta_3 = 60^\circ$; (**b**) for different θ_2 when $\theta_1 = 45^\circ$ and $\theta_3 = 60^\circ$; (**c**) for different v_3 when $v_1 = 1$ cm/year and $v_2 = 1$ cm/year; (**d**) for different distance between the faults F and F_3.

The shear strain accumulation or release rate depends on the depth of faults from the free surface which is described in 8. The rate of shear strain depends on the depth of the point O'' where nonplanarity occurs and its depth from the free surface is $(d_1 + d_2)$. **Figure 8** demonstrates that the rate of shear strain accumulation rises as the depth value decreases. If a fault is situated near the surface, then after the movement of the fault the release of accumulated energy is greater than the fault which is situated at a long distance beneath the surface.

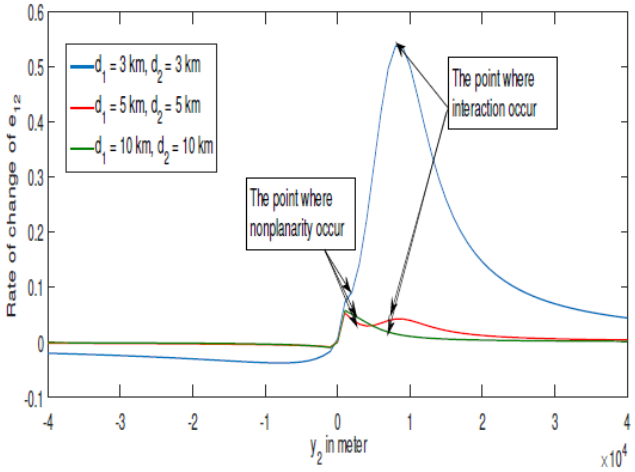

Figure 8. Rate of change of surface shear strain e_{12} with y_2 due to interaction between F and F_3 for different values of depth $(d_1 + d_2)$ of the point O''.

Since the movement of the fault is strike-slip then there is accumulation or release of shear strain on the plane perpendicular to y_1 axis and in y_3 direction and this strain component is defined as e_{13}. The effect of inclination and velocity of the faults on e_{13} have been described in **Figure 9** and **Figure 10**. The rate of e_{13} accumulates across both F and F_3 for different values of θ_1 and θ_2. At $y_2 = 0$, it accumulates maximum value and then falls off. Near $y_2 = 8$ km, i.e when F_3 fault starts to move e_{13} increases again and after attaining maximum value, it decreases towards zero with y_2 increases. The accumulation rate of e_{13} is greater across F than F_3 which is clear from **Figure 9a** and **Figure 9b** respectively. In **Figure 10**, rate of e_{13} has been plotted against y_2 for different creep velocity v_1, v_2 and v_3 is keeping fixed after the movement across both F and F_3. Strain accumulation rate increases with increasing value of velocity.

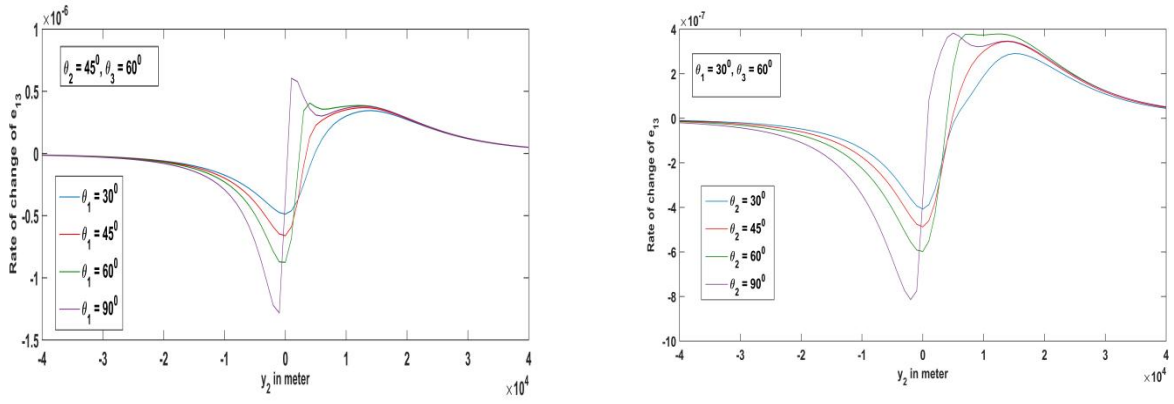

(a) **(b)**

Figure 9. Rate of change of surface strain (e_{13}) with y_2 due to fault creep across both F and F_3. (**a**) for different θ_1 when $\theta_2 = 45°$ and $\theta_3 = 60°$; (**b**) for different θ_2 when $\theta_1 = 30°$ and $\theta_3 = 60°$.

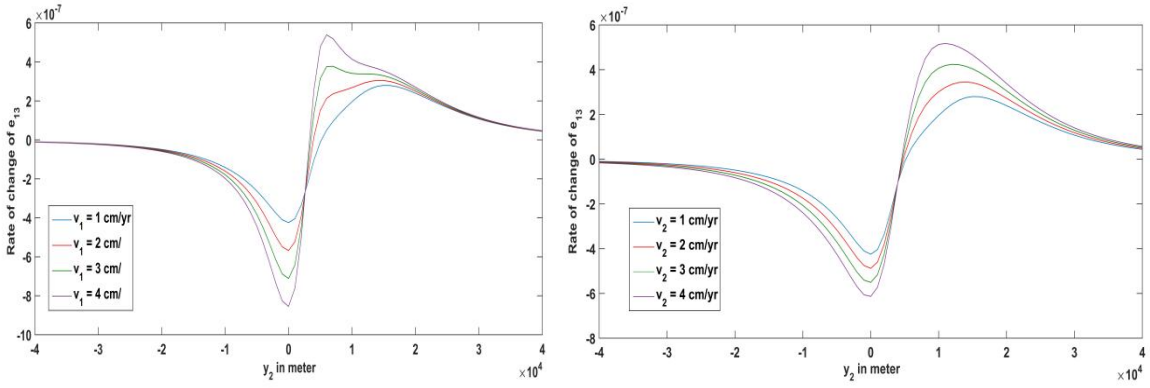

(a) **(b)**

Figure 10. Rate of change of surface strain e_{13} with y_2 due to fault creep across both F and F_3 (**a**) for different v_1 when $v_2 = 1$ cm/year and $v_3 = 1$ cm/year; (**b**) for different v_2 when $v_1 = 1$ cm/year and $v_3 = 1$ cm/year.

The position of the rate of accumulation of maximum strain on the plane perpendicular to y_1 axis and in y_3 direction increase with increasing value of the distance between the faults F and F_3 which is found from **Figure 11**.

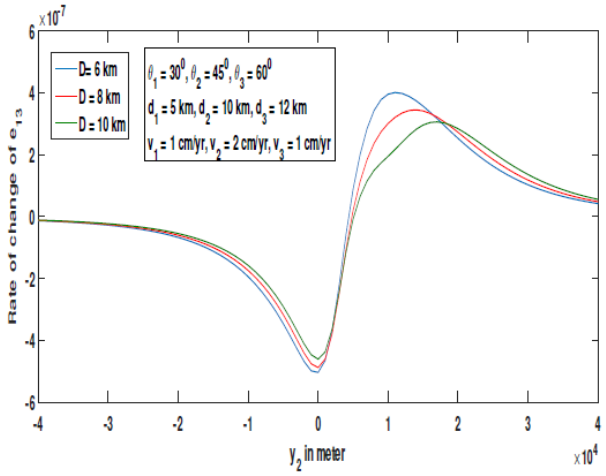

Figure 11. Rate of change of surface strain e_{13} with y_2 due to fault creep across both F and F_3 for different distance between the faults F and F_3.

The rate of change of e_{13} in y_2 direction also depends on width of the faults due to interaction between F and F_3 which has been plotted in **Figure 12**. The rate of release of e_{13} increases with decreasing width of F_1 fault near $y_2 = 0$ and rate of accumulation of e_{13} increases with decreasing width of F_1 near $y_2 = D$ when the width of F_2 and F_3 fixed. Similar variation occurs for different width of F_2 and F_3 when the width of F_1, F_3 fixed and also the width of F_1, F_2 fixed respectively.

The rate of e_{13} also depends on the depth of the faults from the free surface which has been described in **Figure 13**. It is found that e_{13} releases across F and accumulates across F_3. The accumulation and release rate of e_{13} increase with decreasing depth d_1, d_2 and d_3.

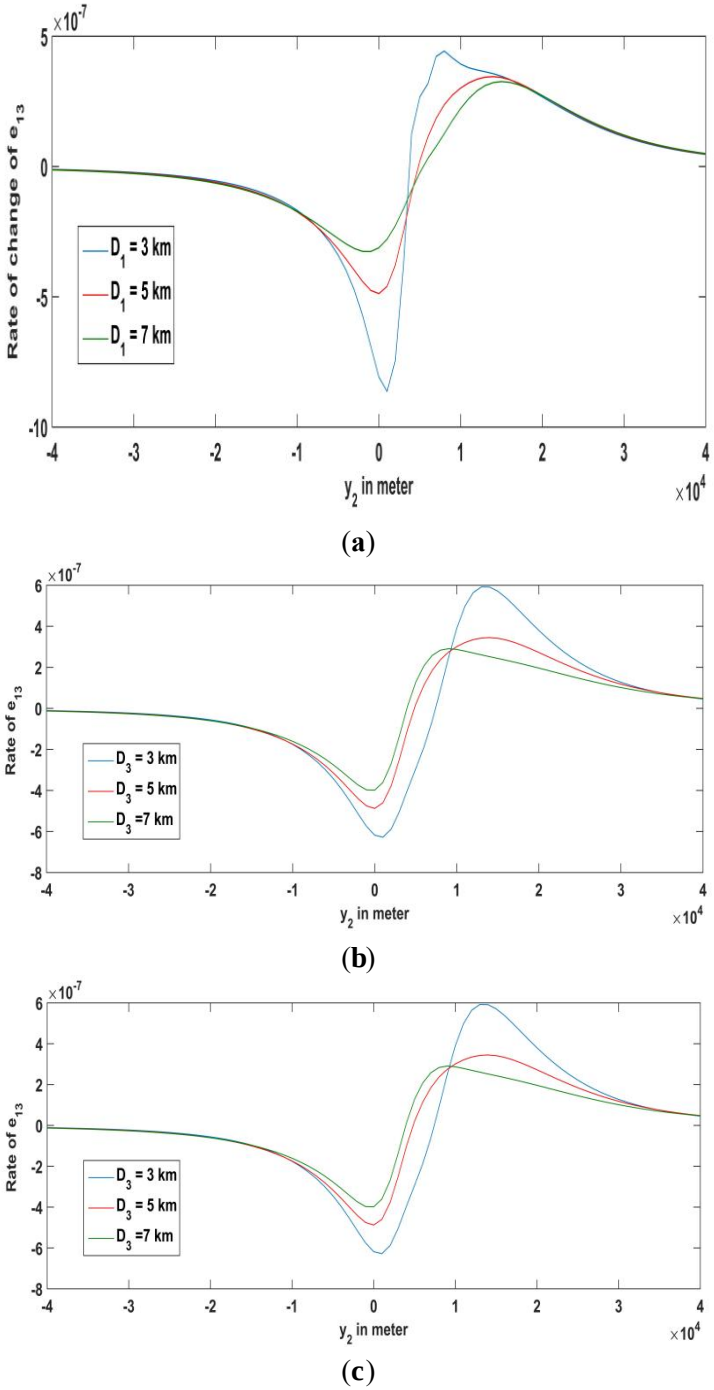

Figure 12. Rate of change of surface strain (e_{13}) with y_2 due to fault creep across both F and F_3. (**a**) for different D_1 when $D_2 = 5$ km and $D_3 = 5$ km; (**b**) for different D_2 when $D_1 = 5$ km and $D_3 = 5$ km; (**c**) for different D_3 when $D_1 = 5$ km and $D_2 = 5$ km.

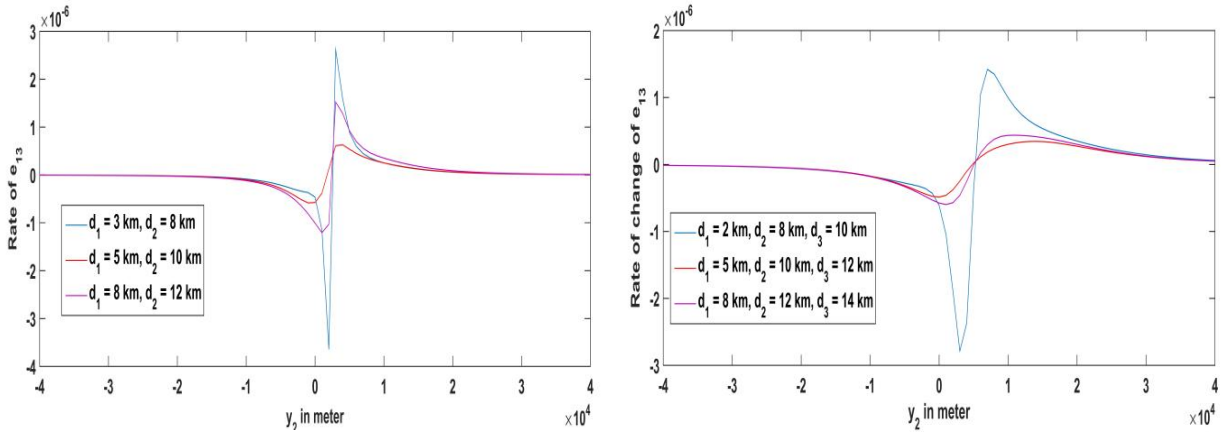

(a) **(b)**

Figure 13. Rate of change of strain (e_{13}) with y_2 due to fault creep across. (**a**) only F (no movement across F_3) for different d_1, d_2; (**b**) both F and F_3 for different d_1, d_2 and d_3.

4.3. Physical Significance of Solutions

(a) Displacement:

- The solutions for displacement show how much the ground moved at the surface and inside the crust due to slip on the faults.
- For nonplanar infinite fault, displacement is not smooth (because the fault bends at point O''. This irregularity reflects how fault bends or changes in dip angle cause localized distortions of the ground.
- The displacement rate is maximum near the first fault segment (F_1) and changes sharply where the fault geometry becomes nonplanar. This helps explain why regions near bends in faults experience stronger ground shaking or deformation.

(b) Stresses: The stress components (τ_{12}, τ_{13}) represent the shear stresses that accumulate and release near the faults.

The solutions show that most stress accumulates in the elastic layer, making it more prone to fault slip compared to the deeper viacoelastic half-space. Nonplanarity alters the distribution at the bend (O''), stress concentration changes slope, which can trigger failure earlier than on planar segments. This is physically important because earthquakes often nucleate at bends, kinks, or fault intersections.

(c) Strains:

- Strain solutions (e_{12}, e_{13}) describe how rocks deform elastically under stress.
- Surface near strain (e_{12}) builds up steadily during the seismic period, then drops sharply during creep.
- Nonplanarity makes the accumulation curve nonsmooth at fault junctions, unlike planar faults where strain accumulation is symmetric.

(d) Interaction effects:

- When the infinite nonplanar fault creeps, stress is transferred to the finite planar fault, potentially triggering its slip later ($T_2 > T_1$).
- This interaction explains sequential faulting in real earthquakes (where one fault's motion triggers another, like in the 2016 Kaikoura earthquake).

4.4. Comparison of Shear Strain Accumulation Rate

If both the non-planar and planar faults are infinite then the variation of shear strain accumulation rate against y_2 has been plotted in **Figure 14a** for $\theta_1 = 60°$, $\theta_2 = 45°$ and $\theta_3 = 60°$. When both the non-planar and planar faults are finite, the change in the rate of shear strain accumulation in the y_2 direction occurs for $\theta_1 = 60°$, $\theta_2 = 45°$ and $\theta_3 = 60°$ has been plotted in **Figure 14b**. In **Figure 14c**, the variation of shear strain accumulation rate against y_2 for infinite non-planar and finite planar fault has been plotted when inclinations are taken as $\theta_1 = 60°$, $\theta_2 = 45°$ and $\theta_3 = 60°$. Comparing **Figure 14c** with **Figure 14a** and **Figure 14b**, it is observed that if both the faults are infinite then the shear strain accumulation rate is greater than one infinite, other fi-

nite faults and which are again greater than both finite faults. It is also analysed that if both the faults are infinite then across F, shear strain accumulates and near F_3, it releases. But when both the faults are finite then shear strain accumulates and after accumulating its maximum value across F_3, it releases towards zero. If the faults are one infinite and the other finite then shear strain accumulates maximum value across the non-planar fault F and then it decreases. After decreasing at a certain level, it increases for $y_2 > 8$ km and for $y_2 > 10$ km, it reduces towards zero. From **Figure 14**, it is concluded that the variation of shear strain accumulation and release due to interaction between two faults is more significant when one fault is infinite and the other is finite, compared to when both faults are either infinite or finite. Since the infinite fault is nonplanar containing two parts then the curve near $y_2 = 0$ that is at the point where fault (F) movement is not smooth whereas if both the faults are planar then the curve is smooth [26].

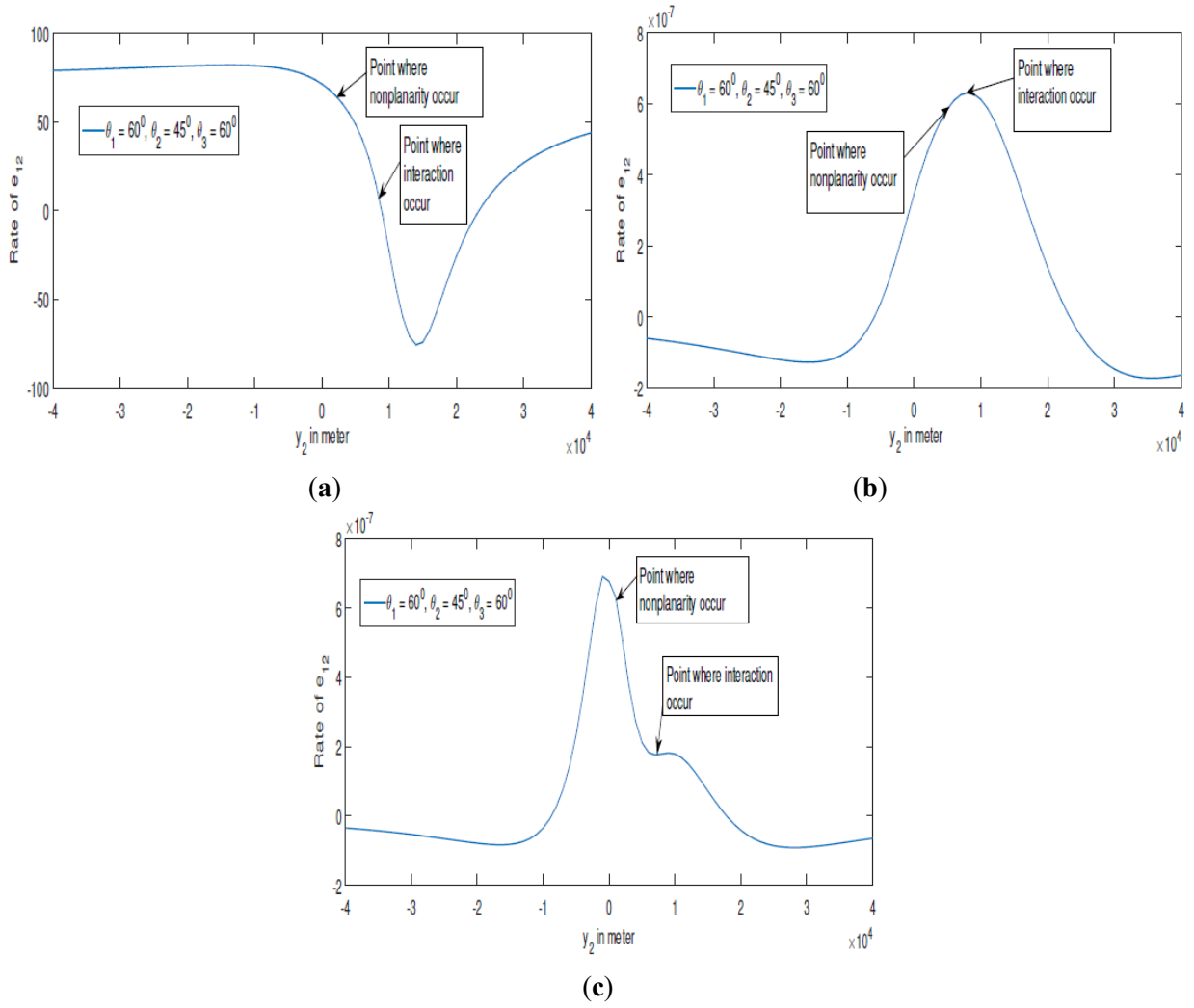

Figure 14. R_{s_2} against y_2 due to fault creep across F and F_3 when (**a**) both the faults are infinite; (**b**) both the faults are finite; (**c**) one infinite and other finite.

4.5. Validation

For ensuring the validity of the obtained results, the present model has been compared with Duan, B. and Oglesby, David D.[14]. Taking the parametric value of viscosity $= 20 \times 10^{21}$, shear modulus $= 3.0 \times 10^{10}$ Pascal, slip $= 0.8$ m, fault element size 500 m.

Comparing **Figure 15a** with **Figure 5** of Duan, B. and Oglesby, David D.[21], it shows that in both the figure the maximum stress threshold that the fault would attain over an infinite period in the absence of seismic activity. Throughout the interseismic period, stresses shift towards the limit level,

with the limit level at a given point dictating whether the stress increases or decreases there. The shear stress rises on the left segment of this fault system but diminishes on the right segment.

If we take the inclination of our nonplanar fault model as 20° then it is observed that in **Figure 15b**, rate of shear stress has been plotted against y_2 (distance from the fault) due to movement across F. Comparing this figure with **Figure 4** of Duan, B. and Oglesby, David D.[21], it is found that for both the cases the shear stress attains its maximum value for $y_2 \to 0^+$ and minimum value for $y_2 \to 0^-$. After attaining the maximum value, for $y_2 > 0$ it decreases towards zero and for $y_2 < 0$ it increases towards zero. The curve of shear stress accumulation and release is a similar type. In Duan, B. and Oglesby, David D.[21] is described that for all different cases, the amount of shear stress accumulation is ≤ 100 MPa. In this paper it is $\leq 3 \times 10^8\ Pa\ (= 300\ MPa)$.

Comparing the amount of stress accumulation of the 2008 MW 7.9 Wenchuan earthquake with our fault model. In the Wenchuan earthquake, the amount of accumulated stress is $1.5 \times 10^4\ \frac{N}{m^2}$ whereas in our fault model, the maximum accumulated shear stress is $2 \times 10^4 \frac{N}{m^2}$.

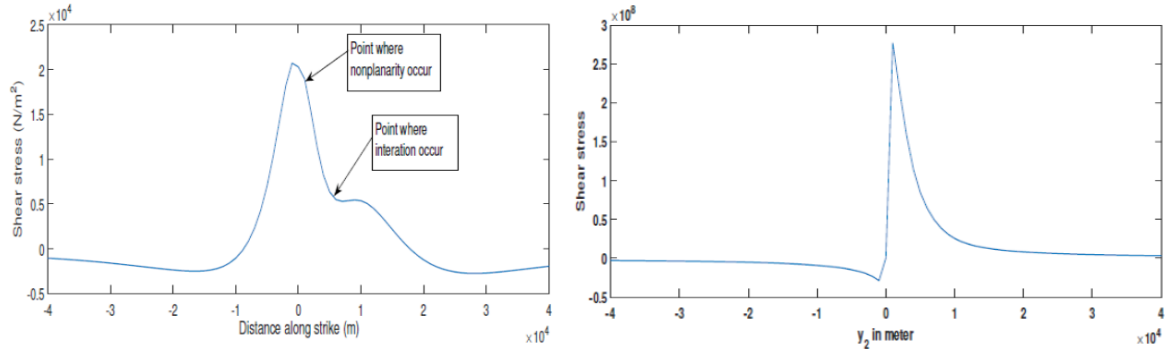

(**a**) (**b**)

Figure 15. (**a**) Shear stress across nonplanar interacting fault model where $\theta_1 = 60^\circ$, $\theta_2 = 30^\circ$ and $\theta_3 = 60^\circ$; (**b**) Shear stress with y_2 due to fault creep across the non-planar fault F only when $\theta_1, \theta_2 = 20^\circ$.

4.6. Quantitative Comparison

To validate the present model, the obtained results are quantitavely compared with with Duan, B. and Oglesby, David D.[21]. The comparison is give below:

- Stress threshold behaviour:
  The present model and Duan, B. and Oglesby, David D.[21] show that the maximum stress threshold is approached asymptotically during the interseismic period. Stress increases on one side of the fault and decreases on the other.
- Shear stress distribution:
  In both studies, shear stress attains a maximum at $y_2 \to 0^+$ and a minimum at $y_2 \to 0^-$. After reaching its maximum value, stress decays towards zero for $y_2 > 0$, and increases towards zero for $y_2 < 0$.
- Magnitude of shear stress accumulation:
  In Duan, B. and Oglesby, David D.[21], the amount of shear stress accumulation is ≤ 100 MPa. In our model, the amount of shear stress accumulation is $\leq 3 \times 10^8$ Pa ≈ 300 MPa.
- Comparison with 2008 Wenchuan earthquake (Mw 7.9):
  The estimated stress accumulation during the 2008 Wenchuan earthquake was approximately$1.5 \times 10^4 N/m^2$. In the present model, the maximum stress accumulation is found to be $2 \times 10^4 N/m^2$ which is clouser to the observed value. This indicates that the proposed fault interaction model captures the stress accumulation mechanism with reasonable accuracy and reflwcts realistic earthquake scenaios.

4.7. Numerical Computation for Earthquake Prediction

From **Figure 16a**, the timing of the next potential fault movement can be estimated. For an example, we can examine a single case with $\theta_1 = 30^\circ$, $\theta_2 = 60^\circ$, $\theta_3 = 30^\circ$ and creep velocities $v_1 = 0.04$ m/year across F_1, $v_2 = 0.02$ m/year across F_2 and $v_3 = 0.02$ m/year across F_3. **Figure 16a** is the graph of the variation of total accumulated stress near the midpoint of F_1 with time t. It is assumed that the

initial stress at $t = 0$ is $(T'_{12})_{0F_1} \approx \frac{1}{6}\sin\theta_1 \approx 25$ bar at $\theta_1 = 30°$. At $T_1 = 50$ years the accumulated stress near F_1 reaches the threshold value $\tau_c = 75$ bar and the fault start to creep. It is presumed that the stress reduces by the same amount due to this movement and returns to its critical value of 25 bar. After the fault undergoes creeping movement, stress starts to rebuild at a diminished rate. It is computed by graphically that T'_{12} near F_1 will again reach threshold level $\tau_c = 75$ bar at $T_1 = 209$ years. Thus, there will be a possible second movement occur after $(209 - 50) = 159$ years. On the other hand, if the stress drops at $t = T_1$ is only 50% of τ_c, a potential second movement could occur at $T_1 = 88$ years i.e after $(88 - 50) = 38$ years from **Figure 16a**.

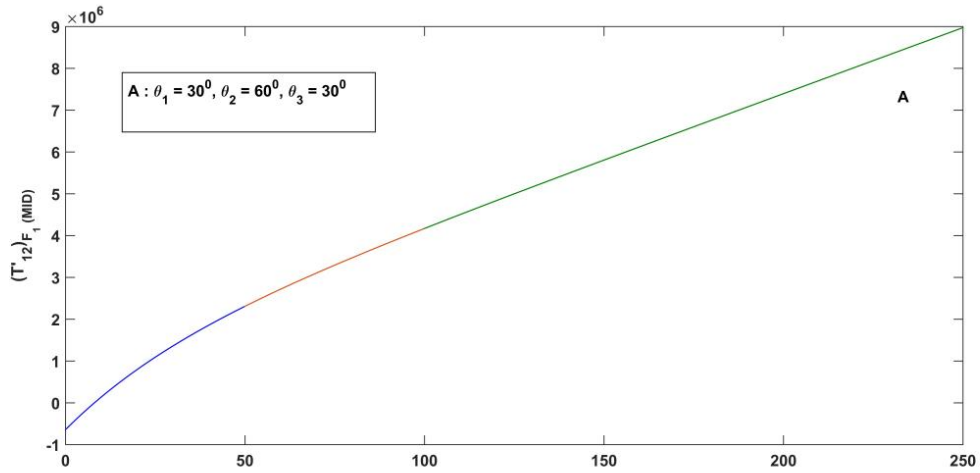

Figure 16. Change of shear stress at the midpoint of F_1 with time when $\theta_1 = 30°$, $\theta_2 = 60°$ and $\theta_3 = 30°$.

5. Key Contributions

- Developed a novel interacting fault model consisting of an infinite nonplanar strike-slip fault and a finite planar strike-slip fault, embedded in an elastic-viscoelastic layered medium.
- Derived closed-form analytical expressions for displacement, stress and strain fields using Laplace transform and Green's function techniques.
- Demostrated the significant influence of nonplanarity on ground deformation , highlighting how dip angles and fault geometry control displacement rates and shear strain accumulation.
- Compared the obtained results with earlier planar fault model (e.g., Kundu and Sarkar[5],) and showed distinct asymmetry introduced by nonplanarity.
- Provided quantitative validation with Duan and Oglesby[21].
- Illustrated the potential application of the model to earthquake harzard estimation, by prediction stress build-up and recurrence intervals under different fault geometries.

6. Conclusions

In this present model, the interaction between a buried, inclined infinite nonplanar fault with a finite, buried planar fault has been considered. The effect of ground deformation on displacement and strain has also been analysed. If the interaction occurs between one infinite and other finite, then its effect is shown more prominent than both infinite or both finite faults.

Comparing with Kundu, P. et al.[4] the difference between the effect of interaction across nonplanar and planar faults with two planar faults has been observed significantly. If both the faults are planar then the displacement rate on the vertical line is smoothly increasing but, in this paper, it is not smoothly increasing because the fault is nonplanar and is contains two parts. Considering the rate of release of surface shear strain per year, it is found that due to interaction between planar faults the curves are symmetrical about a line $y_2 = k$, $k = 0$ for inclination equal to $90°$ and $k > 0$ for $0 < \theta_1, \theta_2 < 90°$. But in this case shear strain is not symmetric $\forall \theta_1, \theta_2$. From the figures it is concluded that at the point O', where nonplanarity occurs, there is

a slight change in the slope of the graph which effects on accumulation of shear strain and also effects on fault displacement. For surface shear stress near the midpoint of F_1 and F_2, movement in each segment affects the overall shear stress accumulation near the other. These attributes are not found in the case of a planar fault. The accumulation rate of shear strain is greater across F than F_3 due to variation of inclinations of the faults with the free surface which indicates that when a fault interacts with other then the amount of release of energy is greater across the first fault than the second fault that is the loss of life or properties is more affected near the first fault than the second fault. When an earthquake occurs at an earthquake-prone site then by investigating the earthquake fault model we can observe the amount of stress-strain accumulation/releases. From this amount of stress-strain accumulation/releases, we can be aware of the occurrence of future earthquakes. The nonplanarity of the fault also effects on rate of displacement and stress-strain accumulation/release.

The present model assumes linear elastic layer over viscoelastic half-space, which may not fully capture the complex non-linear response of real geological materials. The model does not incorporate fluid migration and chemical interactions, which could significantly influence fault zone deformation.

In the present case, the nonplanar fault consists of two planar sub-parts. In future, the number of sub-sections can be expanded, and the related problem can be solved in a comparable way. This study can be extended to incorporate standard linear solid and Burger rheology, in addition to the Maxwell medium and it can be analysed for the model situated in two layers over half-space instead of one layer over half-space. The study can be investigate the effect of temperature, poro-pressure evolution and fluid flow on ground deformation.

Funding

There is no funding for this manuscript. I have applied Institution Contingency Research Grants for this research.

Institutional Review Board Statement

Not applicable.

Informed Consent Statement

Not applicable.

Data Availability Statement

All data generated or analyzed during this study are included in this published article.

Acknowledgments

The author gratefully acknowledges the valuable guidance and suggestions provided by S. Kundu, Assistant Professor, VIT-AP University, Andhra Pradesh, India, during the preparation of this manuscript.

Conflicts of Interest

The author declares no conflict of interest.

Appendix A

The fault F is non-planar containing two parts F_1 and F_2 and F_3 is planar. The displacement, stress, and strain components resulting from the interaction between non-planar and planar faults have been defined in equation (17) to (18) for both layer and half-space. Taking Laplace transform of equations (1) to (8) and all boundary conditions and initial conditions with respect to time t_1, a boundary value problem has been solved involving $(\overline{u_1})_2$, $(\overline{\tau_{12}})_2$, $(\overline{\tau_{13}})_2$ and $(\overline{u_1})_3$, $(\overline{\tau_{12}})_3$, $(\overline{\tau_{13}})_3$ which are Laplace transform of $(u_1)_2$, $(\tau_{12})_2$, $(\tau_{13})_2$ and $(u_1)_3$, $(\tau_{12})_3$, $(\tau_{13})_3$ respectively with respect to time t_1. Therefore

$$\{(\overline{u}_1)_2, (\overline{\tau}_{12})_2, (\overline{\tau}_{13})_2, (\overline{u}_1)_3, (\overline{\tau}_{12})_3, (\overline{\tau}_{13})_3\} = \int_0^\infty \{(u_1)_2, (\tau_{12})_2, (\tau_{13})_2, (u_1)_3, (\tau_{12})_3, (\tau_{13})_3\} e^{-st_1} dt_1$$

where 's' is the variable for Laplace transform variable. The subsequent relations are valid in the transformed domain

$$(\overline{\tau}_{12})_2 + (\overline{\tau}_{12})_3 = \mu_1 \frac{\partial}{\partial y_2} (\overline{u}_1)_2 + \mu_1 \frac{\partial}{\partial y_2} (\overline{u}_1)_3 \quad \text{(A1)}$$

$$(\overline{\tau}_{13})_2 + (\overline{\tau}_{13})_3 = \mu_1 \frac{\partial}{\partial y_3} (\overline{u}_1)_2 + \mu_1 \frac{\partial}{\partial y_3} (\overline{u}_1)_3 \quad \text{(A2)}$$

The displacement component for the elastic layer after fault movement across F is given by (Maruyama[16,17] and Rybicki[15]) $(\overline{u_1})_2(Q) + (\overline{u_1})_3(Q)$ where,

$$(\overline{u}_1)_2(Q) = \int_F [(\overline{u}_1)_2(s)]\,[G_{12}(P,Q)d\xi_3 - G_{13}(P,Q)d\xi_2] \tag{A3}$$

$$(\overline{u}_1)_3(Q) = \int_F [(\overline{u}_1)_3(s)]\,[G_{12}(P,Q)d\xi_3 - G_{13}(P,Q)d\xi_2] \tag{A4}$$

where '$-$' denotes the Laplace transform of a function with respect to time. $P(\xi_1,\xi_2,\xi_3)$ is a point of the fault F and $Q(y_1,y_2,y_3)$ is a field point in elastic layer.

Then $G_{12}(P,Q) = \mu_1 \frac{\partial}{\partial \xi_2} G_1(P,Q)$

$G_{13}(P,Q) = \mu_1 \frac{\partial}{\partial \xi_3} G_1(P,Q)$,

where

$$\begin{aligned} G_1(P,Q) = -\frac{1}{2\pi\mu_3}[&\ln\left\{\sqrt{(\xi_2-y_2)^2+(\xi_3-y_3)^2}\right\} \\ &+ \ln\left\{\sqrt{(\xi_2-y_2)^2+(\xi_3+y_3)^2}\right\} \\ &+ \sum\left(\frac{\mu_1-\mu_2}{\mu_1+\mu_2}\right)^m \\ &(\sqrt{(\xi_2-y_2)^2+(\xi_3-2mH-y_3)^2} \\ &+ \sqrt{(\xi_2-y_2)^2+(\xi_3-2mH+y_3)^2} \\ &+ \sqrt{(\xi_2-y_2)^2+(\xi_3+2mH-y_3)^2} \\ &+ \sqrt{(\xi_2-y_2)^2+(\xi_3+2mH+y_3)^2})] \end{aligned}$$

where $\overline{\mu_2}$ is the Laplace transform of μ_2 with respect to time with $\overline{\mu_2} = \frac{2s+\frac{\mu_2}{\eta}}{\frac{s}{\mu_2}+\frac{1}{\eta}}$, s is the Laplace transform variable and the number of layer is denoted by m and which is taken as 1.

Across F_1, $0 \le \xi_2 \le D_1\cos\theta_1$, $0 \le \xi_3 \le D_1\sin\theta_1$ and $\xi_2 = \xi_3\cot\theta_1$.

A change of co-ordinate axis (ξ_1,ξ_2,ξ_3) to (ξ_1',ξ_2',ξ_3') and $(\xi_1'',\xi_2'',\xi_3'')$ is taken for performing the integration along the fault surface across F_1 and F_2 respectively. Across the fault parts F_1 and F_2 of nonplanar fault F, the co-ordinates (ξ_1,ξ_2,ξ_3) is connected with (ξ_1',ξ_2',ξ_3') and $(\xi_1'',\xi_2'',\xi_3'')$ respectively by the relation

$$\left.\begin{aligned} \xi_1 &= \xi_1' \\ \xi_2 &= \xi_2'\sin\theta_1 + \xi_3'\cos\theta_1 \\ \xi_3 &= -\xi_2'\cos\theta_1 + \xi_3'\sin\theta_1 + d_1 \end{aligned}\right\} \tag{A5}$$

and

$$\left.\begin{aligned} \xi_1 &= \xi_1'' \\ \xi_2 &= D_1\cos\theta_1 + \xi_2''\sin\theta_2 + \xi_3''\cos\theta_2 \\ \xi_3 &= D_1\sin\theta_1 - \xi_2''\cos\theta_2 + \xi_3''\sin\theta_2 + d_1 \end{aligned}\right\} \tag{A6}$$

Using relation $\xi_2 = \xi_3\cot\theta_1$ we get $\xi_2' = 0$ and $\xi_2'' = 0$

Then form equation (A5) and (A6)

$\xi_1 = \xi_1'$

$\xi_2 = \xi_3'\cos\theta_1$

$\xi_3 = \xi_3'\sin\theta_1 + d_1$

and

$\xi_1 = \xi_1''$

$\xi_2 = D_1\cos\theta_1 + \xi_3''\cos\theta_2$

$\xi_3 = D_1\sin\theta_1 + \xi_3''\sin\theta_2 + d_1$

Then from relation (A3) and (A4), it is obtained that

$$(\overline{u}_1)_2(Q) = \frac{U_1(s)}{2\pi}\phi(y_2,y_3) \tag{A7}$$

$$(\overline{u}_1)_3(Q) = \frac{V_1(s)}{2\pi}\psi(y_2,y_3) \tag{A8}$$

where

$$\begin{aligned} \phi = \int_0^{D_1} f(\xi_3')\Bigg[&\frac{y_2\sin\theta_1 - y_3\cos\theta_1 + d_1\cos\theta_1}{A_1} + \frac{y_2\sin\theta_1 + y_3\cos\theta_1 - d_1\cos\theta_1}{A_1} \\ &+ \sum_{m=1}^{\infty}\left(\frac{\mu_1-\mu_2}{\mu_1+\mu_2}\right)^m \left\{\begin{aligned} &\frac{y_2\sin\theta_1 - y_3\cos\theta_1 + d_1\cos\theta_1 - 2mH\cos\theta_1}{A_3} + \frac{y_2\sin\theta_1 + y_3\cos\theta_1 - d_1\cos\theta_1 - 2mH\cos\theta_1}{A_4} \\ &+ \frac{y_2\sin\theta_1 - y_3\cos\theta_1 + d_1\cos\theta_1 + 2mH\cos\theta_1}{A_5} + \frac{y_2\sin\theta_1 + y_3\cos\theta_1 - d_1\cos\theta_1 + 2mH\cos\theta_1}{A_6} \end{aligned}\right\}\Bigg] d\xi_3' \end{aligned}$$

$A_1 = (\xi_3'\cos\theta_1 - y_2)^2 + (\xi_3'\sin\theta_1 - y_3 + d_1)^2$

$A_2 = (\xi_3'\cos\theta_1 - y_2)^2 + (\xi_3'\sin\theta_1 + y_3 - d_1)^2$

$A_3 = (\xi_3'\cos\theta_1 - y_2)^2 + (\xi_3'\sin\theta_1 - 2mH - y_3 + d_1)^2$

$A_4 = (\xi_3'\cos\theta_1 - y_2)^2 + (\xi_3'\sin\theta_1 - 2mH + y_3 - d_1)^2$

$A_5 = (\xi_3'\cos\theta_1 - y_2)^2 + (\xi_3'\sin\theta_1 + 2mH - y_3 + d_1)^2$

$A_6 = (\xi_3'\cos\theta_1 - y_2)^2 + (\xi_3'\sin\theta_1 + 2mH + y_3 - d_1)^2$

and

$$\psi = \int_0^{D_2} f(\xi_3'')\left[\frac{y_2\sin\theta_2 - y_3\cos\theta_2 + (d_1+d_2)\cos\theta_2}{A_1} + \frac{y_2\sin\theta_2 + y_3\cos\theta_2 - (d_1+d_2)\cos\theta_2}{A_1} + \sum_{m=1}^{\infty}\left(\frac{\mu_1-\mu_2}{\mu_1+\mu_2}\right)^m \left\{\begin{array}{l} \dfrac{y_2\sin\theta_2 - y_3\cos\theta_2 + (d_1+d_2)\cos\theta_2 - 2mH\cos\theta_2}{A_3} \\ + \dfrac{y_2\sin\theta_2 + y_3\cos\theta_2 - (d_1+d_2)\cos\theta_2 - 2mH\cos\theta_2}{A_4} \\ + \dfrac{y_2\sin\theta_2 - y_3\cos\theta_2 + (d_1+d_2)\cos\theta_2 + 2mH\cos\theta_2}{A_5} \\ + \dfrac{y_2\sin\theta_2 + y_3\cos\theta_2 - (d_1+d_2)\cos\theta_2 + 2mH\cos\theta_2}{A_6} \end{array}\right\}\right] d\xi_3''$$

$A_1' = (\xi_3''\cos\theta_2 + D_1\cos\theta_1 - y_2)^2 + (\xi_3''\sin\theta_2 + D_1\sin\theta_1 - y_3 + d_2)^2$

$A_2' = (\xi_3''\cos\theta_2 + D_1\cos\theta_1 - y_2)^2 + (\xi_3''\sin\theta_2 + D_1\sin\theta_1 + y_3 - d_2)^2$

$A_3' = (\xi_3''\cos\theta_2 + D_1\cos\theta_1 - y_2)^2 + (\xi_3''\sin\theta_2 + D_1\sin\theta_1 - 2mH - y_3 + d_2)^2$

$A_4' = (\xi_3''\cos\theta_2 + D_1\cos\theta_1 - y_2)^2 + (\xi_3''\sin\theta_2 + D_1\sin\theta_1 - 2mH + y_3 - d_2)^2$

$A_5' = (\xi_3''\cos\theta_2 + D_1\cos\theta_1 - y_2)^2 + (\xi_3''\sin\theta_2 + D_1\sin\theta_1 + 2mH - y_3 + d_2)^2$

$A_6' = (\xi_3''\cos\theta_2 + D_1\cos\theta_1 - y_2)^2 + (\xi_3''\sin\theta_2 + D_1\sin\theta_1 + 2mH + y_3 - d_2)^2$

Taking the inverse Laplace transform on equation (A7) and (A8), displacement across F is

$$(u_1)_2(Q) + (u_1)_3(Q) = \frac{U_1(t_1)}{2\pi}H(t_1)\phi(y_2,y_3) + \frac{V_1(t_1)}{2\pi}H(t_1)\psi(y_2,y_3) \tag{A9}$$

Now from equation (A1) and (A2), it is found that

$(\overline{\tau}_{12})_2 + (\overline{\tau}_{12})_3 = \mu_1\frac{U_1(s)}{2\pi}\phi_2 + \mu_1\frac{V_1(s)}{2\pi}\psi_2$

$(\overline{\tau}_{13})_2 + (\overline{\tau}_{13})_3 = \mu_1\frac{U_1(s)}{2\pi}\phi_3 + \mu_1\frac{V_1(s)}{2\pi}\psi_3$

Taking the inverse Laplace transform it can be expressed as

$(\tau_{12})_2 + (\tau_{12})_3 = \mu_1\frac{U_1(t_1)}{2\pi}\phi_2 + \mu_1\frac{V_1(t_1)}{2\pi}\psi_2$

$(\tau_{13})_2 + (\tau_{13})_3 = \mu_1\frac{U_1(t_1)}{2\pi}\phi_3 + \mu_1\frac{V_1(t_1)}{2\pi}\psi_3$

where $\phi_2 = \frac{\partial\phi}{\partial y_2}$, $\phi_3 = \frac{\partial\phi}{\partial y_3}$, $\psi_2 = \frac{\partial\psi}{\partial y_2}$ and $\psi_3 = \frac{\partial\psi}{\partial y_3}$

Also,

$(\overline{e}_{12})_2 + (\overline{e}_{12})_3 = \frac{U_1(s)}{4\pi}\phi_2 + \frac{V_1(s)}{4\pi}\psi_2$

$(\overline{e}_{13})_2 + (\overline{e}_{13})_3 = \frac{U_1(s)}{4\pi}\phi_3 + \frac{V_1(s)}{4\pi}\psi_3$

Taking the inverse Laplace transform it can be expressed as

$(e_{12})_2 + (e_{12})_3 = \frac{U_1(t_1)}{4\pi}\phi_2 + \frac{V_1(t_1)}{4\pi}\psi_2$

$(e_{13})_2 + (e_{13})_3 = \frac{U_1(t_1)}{4\pi}\phi_3 + \frac{V_1(t_1)}{4\pi}\psi_3$

Similarly due to movement across the finite fault F_3, the field point in elastic layer is $Q_1(z_1,z_2,z_3)$ and a point of the fault F_3 is $P_1(\eta_1,\eta_2,\eta_3)$ then the displacement components after the fault movement is

$$(\overline{u}_1)_4(Q) = \iint_{F_3}\left[(\overline{u}_1)_4(s)\right]\left[G(P_1,Q_1)\right]d\eta_1 d\eta_3 \tag{A10}$$

where $G(P_1,Q_1)$ is greens function satisfy the above boundary value problem and $G(P_1,Q_1) = \frac{\partial}{\partial z_2}G'(P_1,Q_1)$ where

$$G'(P_1,Q_1) = \left[\frac{1}{[(z_1-\eta_1)^2+(z_2-\eta_2)^2+(z_3-\eta_3)^2]^{\frac{1}{2}}} + \frac{1}{[(z_1+\eta_1)^2+(z_2-\eta_2)^2+(z_3-\eta_3)^2]^{\frac{1}{2}}} - \frac{1}{4\pi\mu_1}\sum_{m=1}^{\infty}\left(\frac{\mu_1-\mu_2}{\mu_1+\mu_2}\right)^m \left\{\begin{array}{l} \dfrac{1}{[(z_1-\eta_1)^2+(z_2-\eta_2)^2+(z_3-2mH-\eta_3)^2]^{\frac{1}{2}}} + \dfrac{1}{[(z_1+\eta_1)^2+(z_2-\eta_2)^2+(z_3-2mH+\eta_3)^2]^{\frac{1}{2}}} \\ + \dfrac{1}{[(z_1-\eta_1)^2+(z_2-\eta_2)^2+(z_3+2mH+\eta_3)^2]^{\frac{1}{2}}} + \dfrac{1}{[(z_1-\eta_1)^2+(z_2-\eta_2)^2+(z_3+2mH-\eta_3)^2]^{\frac{1}{2}}} \end{array}\right\}\right]$$

where

$z_1 = y_1$, $z_2 = y_2 - D$, $z_3 = y_3 - d_1 - d_2$

A change of co-ordinate from (η_1,η_2,η_3) to $(\xi_1''',\xi_2''',\xi_3''')$ is connected by the relation

$$\left.\begin{aligned}\eta_1 &= \xi_1^{'''}\\ \eta_2 &= \xi_2^{'''}\sin\theta_3 + \xi_3^{'''}\cos\theta_3\\ \eta_3 &= -\xi_2^{'''}\sin\theta_3 + \xi_3^{'''}\cos\theta_3\end{aligned}\right\} \tag{A11}$$

Using the relation $\eta_2 = \eta_3\cot\theta_3$ we get, $\xi_2^{'''} = 0$,

Then from equation (41), $\eta_1 = \xi_1^{'''}$, $\eta_2 = \xi_3^{'''}\cos\theta_3$, $\eta_3 = \xi_3^{'''}\cos\theta_3$

Then displacement across F_3 is

$$(\overline{u}_1)_4(Q) = \int_{-L}^{L}\int_0^{D_3}[(\overline{u}_1)_4(s)]\,G(P_1,Q_1)d\xi_1^{'''}d\xi_3^{'''} \tag{A12}$$

Then $(\overline{u}_1)_4(Q) = \frac{U_2(s)}{2\pi}\chi(y_1,y_2,y_3)$

Taking inverse Laplace transform we get $(u_1)_4 = \frac{U_2(t_2)}{2\pi}H(t_2)\chi(y_1,y_2,y_3)$, where $t_2 = t - T_2$

where $\chi(y_1,y_2,y_3) =$

$$\begin{aligned}\chi(y_1,y_2,y_3) = \int_{-L}^{L}\int_0^{D_3}\Bigg[&\frac{y_2-D-\xi_3^{'''}\cos\theta_3}{\{(y_1-\xi_1^{'''})^2+(y_2-D-\xi_3^{'''}\cos\theta_3)^2+(y_3-d_1-d_2-\xi_3^{'''}\sin\theta_3)^2\}^{\frac{3}{2}}}\\ &+\frac{y_2-D-\xi_3^{'''}\cos\theta_3}{\{(y_1+\xi_1^{'''})^2+(y_2-D-\xi_3^{'''}\cos\theta_3)^2+(y_3-d_1-d_2-\xi_3^{'''}\sin\theta_3)^2\}^{\frac{3}{2}}}\\ &-\frac{1}{4\pi\mu_1}\sum_{m=1}^{\infty}\left(\frac{\mu_1-\mu_2}{\mu_1+\mu_2}\right)^m\left\{\begin{aligned}&\frac{y_2-D-\xi_3^{'''}\cos\theta_3}{\{(y_1-\xi_1^{'''})^2+(y_2-D-\xi_3^{'''}\cos\theta_3)^2+(y_3-d_1-d_2-2mH-\xi_3^{'''}\sin\theta_3)^2\}^{\frac{3}{2}}}\\ &+\frac{y_2-D-\xi_3^{'''}\cos\theta_3}{\{(y_1-\xi_1^{'''})^2+(y_2-D-\xi_3^{'''}\cos\theta_3)^2+(y_3-d_1-d_2+2mH+\xi_3^{'''}\sin\theta_3)^2\}^{\frac{3}{2}}}\\ &+\frac{y_2-D-\xi_3^{'''}\cos\theta_3}{\{(y_1-\xi_1^{'''})^2+(y_2-D-\xi_3^{'''}\cos\theta_3)^2+(y_3-d_1-d_2+2mH-\xi_3^{'''}\sin\theta_3)^2\}^{\frac{3}{2}}}\end{aligned}\right\}\Bigg]f(\xi_1^{'''},\xi_3^{'''})d\xi_1^{'''}d\xi_3^{'''}\end{aligned}$$

Therefore $(\overline{\tau}_{11})_4 = 2\mu_1\frac{U_2(s)}{2\pi}\chi_1(y_1,y_2,y_3)$

$(\overline{\tau}_{12})_4 = 2\mu_1\frac{U_2(s)}{2\pi}\chi_2(y_1,y_2,y_3)$

$(\overline{\tau}_{13})_4 = 2\mu_1\frac{U_2(s)}{2\pi}\chi_3(y_1,y_2,y_3)$

Taking inverse Laplace transform we get

$(\tau_{11})_4 = 2\mu_1\frac{U_2(t_2)}{2\pi}\chi_1(y_1,y_2,y_3)$

$(\tau_{12})_4 = 2\mu_1\frac{U_2(t_2)}{2\pi}\chi_2(y_1,y_2,y_3)$

$(\tau_{13})_4 = 2\mu_1\frac{U_2(t_2)}{2\pi}\chi_3(y_1,y_2,y_3)$

Also $(e_{12})_4 = \frac{U_2(t_2)}{4\pi}\chi_2$ and $(e_{13})_4 = \frac{U_2(t_2)}{4\pi}\chi_3$

where $\chi_1 = \frac{\partial\chi}{\partial y_1}$, $\chi_2 = \frac{\partial\chi}{\partial y_2}$, $\chi_3 = \frac{\partial\chi}{\partial y_3}$

Appendix B

Now for viscoelastic half-space ($y_3 > H$), the displacement component after the fault movement across F is

$$(\overline{u}_1')_2(Q) + (\overline{u}_1')_3(Q)$$

where

$$(\overline{u}_1')_2(Q) = \int_F[(\overline{u}_1')_2(s)]\,[G_{12}'(P,Q)d\xi_3 - G_{13}'(P,Q)d\xi_2] \tag{A13}$$

where '-' denote the Laplace transform of a function with respect to time.

$P(\xi_1,\xi_2,\xi_3)$ is a point across F and $Q(y_1,y_2,y_3)$ is a field point in elastic layer.

Then $G_{12}'(P,Q) = \mu_1\frac{\partial}{\partial\xi_2}G_1'(P,Q)$

$G_{13}'(P,Q) = \mu_1\frac{\partial}{\partial\xi_3}G_1'(P,Q)$,

where

$$\begin{aligned}G_1'(P,Q) = -\frac{1}{\pi(\mu_1+\mu_2)}\Bigg[&\ln\sqrt{(\xi_2-y_2)^2+(\xi_3-y_3)^2}+\ln\sqrt{(\xi_2-y_2)^2+(\xi_3+y_3)^2}\\ &+\sum\left(\frac{\mu_1-\mu_2}{\mu_1+\mu_2}\right)^m\Big(\sqrt{(\xi_2-y_2)^2+(\xi_3-2mH-y_3)^2}+\sqrt{(\xi_2-y_2)^2+(\xi_3-2mH+y_3)^2}\\ &+\sqrt{(\xi_2-y_2)^2+(\xi_3+2mH-y_3)^2}+\sqrt{(\xi_2-y_2)^2+(\xi_3+2mH+y_3)^2}\Big)\Bigg]\end{aligned}$$

Therefore $(\overline{u}_1')_2(Q) = \frac{U_1(s)}{2\pi}\phi'(y_2, y_3)$

Taking inverse Laplace transform,

$$(u_1')_2(Q) = \frac{U_1(t_1)}{2\pi}\phi'(y_2, y_3) \tag{A14}$$

where

$$\begin{aligned}\phi' = \frac{\mu_1}{\mu_1+\mu_2}\int_0^{D_1} f(\xi_3')\Bigg[&\frac{y_2\sin\theta_1 - y_3\cos\theta_1 + d_1\cos\theta_1}{A_1} + \frac{y_2\sin\theta_1 + y_3\cos\theta_1 - d_1\cos\theta_1}{A_1}\\ &+\sum_{m=1}^{\infty}\left(\frac{\mu_1-\mu_2}{\mu_1+\mu_2}\right)^m\left\{\begin{array}{l}\dfrac{y_2\sin\theta_1 - y_3\cos\theta_1 + d_1\cos\theta_1 - 2mH\cos\theta_1}{A_3} + \dfrac{y_2\sin\theta_1 + y_3\cos\theta_1 - d_1\cos\theta_1 - 2mH\cos\theta_1}{A_4}\\ +\dfrac{y_2\sin\theta_1 - y_3\cos\theta_1 + d_1\cos\theta_1 + 2mH\cos\theta_1}{A_5} + \dfrac{y_2\sin\theta_1 + y_3\cos\theta_1 - d_1\cos\theta_1 + 2mH\cos\theta_1}{A_6}\end{array}\right\}\Bigg]d\xi_3'\end{aligned} \tag{A15}$$

$$\begin{aligned}A_1 &= (\xi_3'\cos\theta_1 - y_2)^2 + (\xi_3'\sin\theta_1 - y_3 + d_1)^2\\ A_2 &= (\xi_3'\cos\theta_1 - y_2)^2 + (\xi_3'\sin\theta_1 + y_3 - d_1)^2\\ A_3 &= (\xi_3'\cos\theta_1 - y_2)^2 + (\xi_3'\sin\theta_1 - 2mH - y_3 + d_1)^2\\ A_4 &= (\xi_3'\cos\theta_1 - y_2)^2 + (\xi_3'\sin\theta_1 - 2mH + y_3 - d_1)^2\end{aligned}$$

$$\begin{aligned}A_5 &= (\xi_3'\cos\theta_1 - y_2)^2 + (\xi_3'\sin\theta_1 + 2mH - y_3 + d_1)^2\\ A_6 &= (\xi_3'\cos\theta_1 - y_2)^2 + (\xi_3'\sin\theta_1 + 2mH + y_3 - d_1)^2\end{aligned}$$

and

$$(u_1')_3(Q) = \frac{V_1(t_1)}{2\pi}\psi'(y_2, y_3) \tag{A16}$$

$$\begin{aligned}\psi' = \frac{\mu_1}{\mu_1+\mu_2}\int_0^{D_2} f(\xi_3'')\Bigg[&\frac{y_2\sin\theta_2 - y_3\cos\theta_2 + (d_1+d_2)\cos\theta_2}{A_1}\\ &+\frac{y_2\sin\theta_2 + y_3\cos\theta_2 - (d_1+d_2)\cos\theta_2}{A_1}\\ &+\sum_{m=1}^{\infty}\left(\frac{\mu_1-\mu_2}{\mu_1+\mu_2}\right)^m\left\{\begin{array}{l}\dfrac{y_2\sin\theta_2 - y_3\cos\theta_2 + (d_1+d_2)\cos\theta_2 - 2mH\cos\theta_2}{A_3}\\ +\dfrac{y_2\sin\theta_2 + y_3\cos\theta_2 - (d_1+d_2)\cos\theta_2 - 2mH\cos\theta_2}{A_4}\\ +\dfrac{y_2\sin\theta_2 - y_3\cos\theta_2 + (d_1+d_2)\cos\theta_2 + 2mH\cos\theta_2}{A_5}\\ +\dfrac{y_2\sin\theta_2 + y_3\cos\theta_2 - (d_1+d_2)\cos\theta_2 + 2mH\cos\theta_2}{A_6}\end{array}\right\}\Bigg]d\xi_3''\end{aligned}$$

$$\begin{aligned}A_1' &= (\xi_3''\cos\theta_2 + D_1\cos\theta_1 - y_2)^2 + (\xi_3''\sin\theta_2 + D_1\sin\theta_1 - y_3 + d_2)^2\\ A_2' &= (\xi_3''\cos\theta_2 + D_1\cos\theta_1 - y_2)^2 + (\xi_3''\sin\theta_2 + D_1\sin\theta_1 + y_3 - d_2)^2\\ A_3' &= (\xi_3''\cos\theta_2 + D_1\cos\theta_1 - y_2)^2 + (\xi_3''\sin\theta_2 + D_1\sin\theta_1 - 2mH - y_3 + d_2)^2\\ A_4' &= (\xi_3''\cos\theta_2 + D_1\cos\theta_1 - y_2)^2 + (\xi_3''\sin\theta_2 + D_1\sin\theta_1 - 2mH + y_3 - d_2)^2\\ A_5' &= (\xi_3''\cos\theta_2 + D_1\cos\theta_1 - y_2)^2 + (\xi_3''\sin\theta_2 + D_1\sin\theta_1 + 2mH - y_3 + d_2)^2\\ A_6' &= (\xi_3''\cos\theta_2 + D_1\cos\theta_1 - y_2)^2 + (\xi_3''\sin\theta_2 + D_1\sin\theta_1 + 2mH + y_3 - d_2)^2\end{aligned}$$

Taking inverse Laplace transform, displacement across F is

$$\begin{aligned}(u_1')_2(Q) + (u_1')_3(Q) = &\frac{U_1(t_1)}{2\pi}H(t_1)\phi'(y_2, y_3)\\ &+\frac{V_1(t_1)}{2\pi}H(t_1)\psi'(y_2, y_3)\end{aligned} \tag{A17}$$

Now

$$\begin{aligned}(\tau_{12}')_2 + (\tau_{12}')_3 &= \mu_1\tfrac{U_1(t_1)}{2\pi}\phi_2' + \mu_1\tfrac{V_1(t_1)}{2\pi}\psi_2'\\ (\tau_{13}')_2 + (\tau_{13}')_3 &= \mu_1\tfrac{U_1(t_1)}{2\pi}\phi_3' + \mu_1\tfrac{V_1(t_1)}{2\pi}\psi_3'\\ (e_{12}')_2 + (e_{12}')_3 &= \tfrac{U_1(t_1)}{4\pi}\phi_2' + \tfrac{V_1(t_1)}{4\pi}\psi_2'\\ (e_{13}')_2 + (e_{13}')_3 &= \tfrac{U_1(t_1)}{4\pi}\phi_3' + \tfrac{V_1(t_1)}{4\pi}\psi_3'\end{aligned}$$

where $\phi_2' = \frac{\partial\phi'}{\partial y_2}$, $\phi_3' = \frac{\partial\phi'}{\partial y_3}$, $\psi_2' = \frac{\partial\psi'}{\partial y_2}$ and $\psi_3' = \frac{\partial\psi'}{\partial y_3}$

The displacement components after the fault movement due to movement across the finite fault F_3 is

$(u_1')_4 = \frac{U_2(t_2)}{2\pi}H(t_2)\chi(y_1, y_2, y_3)$, where $t_2 = t - T_2$

where $\chi'(y_1, y_2, y_3) =$

$$
- \frac{\mu_1}{\mu_1+\mu_2}\int_{-L}^{L}\int_{0}^{D_3}\Bigg[\frac{y_2-D-\xi_3'''\cos\theta_3}{\{(y_1-\xi_1''')^2+(y_2-D-\xi_3'''\cos\theta_3)^2+(y_3-d_1-d_2-\xi_3'''\sin\theta_3)^2\}^{\frac{3}{2}}}
$$

$$
+\frac{y_2-D-\xi_3'''\cos\theta_3}{\{(y_1+\xi_1''')^2+(y_2-D-\xi_3'''\cos\theta_3)^2+(y_3-d_1-d_2-\xi_3'''\sin\theta_3)^2\}^{\frac{3}{2}}}
$$

$$
-\frac{1}{4\pi\mu_1}\sum_{m=1}^{\infty}\left(\frac{\mu_1-\mu_2}{\mu_1+\mu_2}\right)^m\left\{\begin{array}{l}\dfrac{y_2-D-\xi_3'''\cos\theta_3}{\{(y_1-\xi_1''')^2+(y_2-D-\xi_3'''\cos\theta_3)^2+(y_3-d_1-d_2-2mH-\xi_3'''\sin\theta_3)^2\}^{\frac{3}{2}}}\\ +\dfrac{y_2-D-\xi_3'''\cos\theta_3}{\{(y_1-\xi_1''')^2+(y_2-D-\xi_3'''\cos\theta_3)^2+(y_3-d_1-d_2-2mH+\xi_3'''\sin\theta_3)^2\}^{\frac{3}{2}}}\\ +\dfrac{y_2-D-\xi_3'''\cos\theta_3}{\{(y_1-\xi_1''')^2+(y_2-D-\xi_3'''\cos\theta_3)^2+(y_3-d_1-d_2+2mH+\xi_3'''\sin\theta_3)^2\}^{\frac{3}{2}}}\\ +\dfrac{y_2-D-\xi_3'''\cos\theta_3}{\{(y_1-\xi_1''')^2+(y_2-D-\xi_3'''\cos\theta_3)^2+(y_3-d_1-d_2+2mH-\xi_3'''\sin\theta_3)^2\}^{\frac{3}{2}}}\end{array}\right\}\Bigg]f(\xi_1''',\xi_3''')d\xi_1'''d\xi_3'''
$$

$$(\tau'_{11})_4 = 2\mu_1\frac{U_2(t_2)}{2\pi}\chi'_1(y_1,y_2,y_3)$$
$$(\tau'_{12})_4 = 2\mu_1\frac{U_2(t_2)}{2\pi}\chi'_2(y_1,y_2,y_3)$$
$$(\tau'_{13})_4 = 2\mu_1\frac{U_2(t_2)}{2\pi}\chi'_3(y_1,y_2,y_3)$$

Also $(e'_{12})_4 = \frac{U_2(t_2)}{4\pi}\chi'_2$ and $(e'_{13})_4 = \frac{U_2(t_2)}{4\pi}\chi'_3$ where $\chi'_1 = \frac{\partial\chi'}{\partial y_1},\ \chi'_2 = \frac{\partial\chi'}{\partial y_2},\ \chi'_3 = \frac{\partial\chi'}{\partial y_3}$.

References

[1] Gabbianelli, G., Rapone, A., Milanesi, R.R., et al., 2025. Impact of Far- and Near-Field Records on the Seismic Fragility of Steel Storage Tanks. Applied Mechanics. 6(2), 24. DOI: https://doi.org/10.3390/applmech6020024

[2] Liu, Y., Erten, E. & Gonzalez-Ortega, A., et al., 2025. Shear-strain evolution in the East Anatolian Fault Zone revealed by InSAR phase gradients after the 2020 Elazig and 2023 kahramanmaras earthquakes. Geophysical Research Letters, 52(4). DOI: 10.1029/2024GL114033

[3] Mahato, P., Sarkar Mondal, S., 2025. Effect on surface deformation due to interacting fault in fractional standard linear solid. GEM—International Journal on Geomathematics. 16(1), 5. DOI: https://doi.org/10.1007/s13137-025-00264-5

[4] Kundu, P., 2024. On the Investigation of Interacting Fault Movement in a Viscoelastic Structure. In: Saha, A., Banerjee, S. (eds.). Proceedings of the 2nd International Conference on Nonlinear Dynamics and Applications (ICNDA 2024), Volume 2. Springer Nature: Cham, Switzerland; pp. 560–575. DOI: https://doi.org/10.1007/978-3-031-69134-8_39

[5] Kundu, P., Sarkar, S., 2020. Deformation analysis of a viscoelastic half-space due to a finite and an infinite interacting faults. Physica Scripta. 95(5), 055004. DOI: https://doi.org/10.1088/1402-4896/ab6f94

[6] Mondal, D., Kundu, P., Sarkar, S., 2020. Accumulation of Stress and Strain due to an Infinite Strike-Slip Fault in an Elastic Layer Overlying a Viscoelastic Half Space of Standard Linear Solid (SLS). Pure and Applied Geophysics. 177(10), 4643–4656. DOI: https://doi.org/10.1007/s00024-020-02536-7

[7] Muir, C., Cortez, J., Grigolini, P., 2020. Interacting faults in california and hindu kush. Chaos, Solitons & Fractals. 139, 110070. DOI: https://doi.org/10.1016/j.chaos.2020.110070

[8] Dutta, R., Jónsson, S., Vasyura-Bathke, H., 2021. Simultaneous Bayesian Estimation of Non-Planar Fault Geometry and Spatially-Variable Slip. Journal of Geophysical Research: Solid Earth. 126(7), e2020JB020441. DOI: https://doi.org/10.1029/2020JB020441

[9] Li, D., Liu, Y., 2016. Spatiotemporal evolution of slow slip events in a nonplanar fault model for northern Cascadia subduction zone. Journal of Geophysical Research: Solid Earth. 121(9), 6828–6845. DOI: https://doi.org/10.1002/2016JB012857

[10] Sen, S., Karmakar, A., Mondal, B., 2012. A nonplanar surface breaking strike slip fault in a viscoelastic half space model of the lithosphere. IOSR Journal Of Mathematics. 2, 32–46, DOI: https://doi.org/10.9790/5728-0253246

[11] Marshall, S.T., Cooke, M.L., Owen, S.E., 2008. Effects of Nonplanar Fault Topology and Mechanical Interaction on Fault-Slip Distributions in the Ventura Basin, California. Bulletin of the Seismological Society of America. 98(3), 1113–1127. DOI: https://doi.org/10.1785/0120070159

[12] Mitsui, N., Hirahara, K., 2006. Slow slip events controlled by the slab dip and its lateral change along a trench. Earth and Planetary Science Letters. 245(1–2), 344–358. DOI: https://doi.org/10.1016/j.epsl.2006.03.001

[13] Rani, S., Singh, S.J., 1992. Static deformation of a uniform half-space due to a long dip-slip fault. Geophysical Journal International. 109(2), 469–476. DOI: https://doi.org/10.1111/j.1365-246X.1992.tb00108.x

[14] Rani, S., Singh, S.J., Garg, N.R., 1991. Displacements and stresses at any point of a uniform half-space due to two-dimensional buried sources. Physics of the Earth and Planetary Interiors. 65(3–5), 276–282. DOI:

https://doi.org/10.1016/0031-9201(91)90134-4

[15] Rybicki, K., 1971. The elastic residual field of a very long strike-slip fault in the presence of a discontinuity. Bulletin of the Seismological Society of America. 61(1), 79–92. DOI: https://doi.org/10.1785/BSSA0610010079

[16] Maruyam, T., 1966. On two-dimensional dislocation in an infinite and semi-infinite medium. Bull. Earthquake Research Institute. 44, 811–871.

[17] Maruyama, T., 1964. Static elastic dislocations in an infinite and semi-infinite medium. Bull. Earthquake Research Institute. 42, 289–368.

[18] Chinnery, M.A., 1963. The stress changes that accompany strike-slip faulting. Bulletin of the Seismological Society of America. 53(5), 921–932. DOI: https://doi.org/10.1785/BSSA0530050921

[19] Chinnery, M.A., 1961. The deformation of the ground around surface faults. Bulletin of the Seismological Society of America. 51(3), 355–372. DOI: https://doi.org/10.1785/BSSA0510030355

[20] Steketee, J.A., 1958. SOME GEOPHYSICAL APPLICATIONS OF THE ELASTICITY THEORY OF DISLOCATIONS. Canadian Journal of Physics. 36(9), 1168–1198. DOI: https://doi.org/10.1139/p58-123

[21] Duan, B., Oglesby, D.D., 2005. Multicycle dynamics of nonplanar strike-slip faults. Journal of Geophysical Research: Solid Earth. 110(B3), 2004JB003298. DOI: https://doi.org/10.1029/2004JB003298

[22] Ghosh, U., Mukhopadhyay, A., Sen, S., 1992. On two interacting creeping vertical surface-breaking strike-slip faults in a two-layer model of the lithosphere. Physics of the Earth and Planetary Interiors. 70(1–2), 119–129. DOI: https://doi.org/10.1016/0031-9201(92)90166-S

[23] Cathles, L.M., 1975. The visco-elasticity of the earth's mantle. Princeton University Press: Princeton, NJ, USA.

[24] Aki, K., Richards, P.G., 1980. Quantitative seismology: Theory and methods. WH Freeman: New York, NY, USA.

[25] Clift, P., Lin, J., Barckhausen, U., 2002. Evidence of low flexural rigidity and low viscosity lower continental crust during continental break-up in the South China Sea. Marine and Petroleum Geology. 19(8), 951–970. DOI: https://doi.org/10.1016/S0264-8172(02)00108-3

[26] Karato, S., 2010. Rheology of the Earth's mantle: A historical review. Gondwana Research. 18(1), 17–45. DOI: https://doi.org/10.1016/j.gr.2010.03.004

[27] Savage, J.C., Burford, R.O., 1970. Accumulation of tectonic strain in California. Bulletin of the Seismological Society of America. 60(6), 1877–1896. DOI: https://doi.org/10.1785/BSSA0600061877